Proposal and experimental validation of simplified strut-and-tie models on dapped-end beams

Jaime Mata-Falcón[a,1]; Luis Pallarés[a]; Pedro F. Miguel[a]

[a]Institute of Concrete Science and Technology (ICITECH) - Universitat Politècnica de València (UPV) – Camino de Vera s/n – 46022 Valencia, Spain

[1]Corresponding author: Tel.: +41 44 633 31 63; Email: mata-falcon@ibk.baug.ethz.ch; Present address: ETH Zurich, Chair of Structural Engineering: Concrete Structures and Bridge Design, Stefano-Franscini-Platz 5, 8093 Zürich, Switzerland

Highlights

Dapped-end beams present spalling issues on top of hanger reinforcement.

Twenty-eight tests on fifteen different reinforcement configurations are presented.

Strut-and-tie models deduced from the experimental results are presented.

A simplified strut-and-tie model for dapped-end beams is proposed.

The model is verified with experimental data including data from the literature.

Abstract

Dapped-end beams are frequent precast concrete elements. Spalling on the top of the hanger reinforcement has been observed to be often their governing failure mode. This failure hinders the geometric definition of strut-and-tie models for design or assessment purposes. In this work, a simplified procedure for defining the geometry of strut-and-tie models considering spalling failures is proposed. The model is based on the results of a specific experimental programme consisting on twenty-eight tests on fifteen different reinforcement configurations with and without inclined reinforcement. The experimental results show that elements with high amounts of reinforcement and hanger reinforcement concentrated in one layer are more prone to spalling failures, and suggest that the geometry of strut-and-tie models is strongly influenced by the behaviour of the nodal region on top of the hanger reinforcement. The model is verified for tests with and without spalling failures, including elements from the literature, showing sound agreement between the modelling results and experimental observations.

Proposal and experimental validation of simplified strut-and-tie models on dapped-end beams

by Jaime Mata-Falcón, Luis Pallarés and Pedro F. Miguel

Keywords

Concrete Structures; Dapped-end beams; Half joints; Experimental analysis; Spalling; Limit analysis; Strut-and-tie models; Simplified formulations

Notation

Greek letters

β_D angle of diagonal dapped-end reinforcement

ε_{si} strain of reinforcement "*si*", where si={sD; sH; $sV1$; $sV2$ or $sV3$}

δ displacement in the centre of the beam

δ_{peak} displacement in the centre of the beam at peak load

λ_c dimensionless coefficient of the proposed model relating the concrete capacity and the element's horizontal capacity

λ_d dimensionless coefficient of the proposed model relating the diagonal reinforcement's capacity and the element's horizontal capacity

Lowercase Latin letters

a_3 horizontal separation of the beam shear tie to the strut-and-tie node over the support

a_D horizontal separation of the diagonal dapped-end tie to the strut-and-tie node over the support

a_V horizontal separation of the vertical dapped-end tie to the strut-and-tie node over the support

b dapped-end beam width

d effective depth in the nib (distance from the centroid of the horizontal dapped-end reinforcement to the outermost compressed fibre)

f_c concrete cylinder compressive strength

f_y reinforcement yield strength

f_u reinforcement ultimate strength

k_c concrete strength reduction factor (due to the transversal strain state and increasing brittleness with strength)

sD diagonal dapped-end reinforcement

$sF1$ bottom layer of beam flexural reinforcement

$sF2$ second layer of beam flexural reinforcement

sH horizontal dapped-end reinforcement

sT beam shear reinforcement

sV vertical dapped-end reinforcement, also referred to as hanger reinforcement

$sV1$ first stirrup of the vertical dapped-end reinforcement

$sV2$ second stirrup of the vertical dapped-end reinforcement

$sV3$ third stirrup of the vertical dapped-end reinforcement

x distance between the strut-and-tie node on top of the hanger reinforcement and the outermost compressed fibre

z distance between the strut-and-tie node on top of the hanger reinforcement and the centroid of the horizontal dapped-end reinforcement

Uppercase Latin letters

A_{si} total cross-sectional area of reinforcement "*si*", where si={ sD; $sF1$; $sF2$; sH; sT or sV}

H horizontal force at the dapped-end

L_{sD} horizontal segment length of the diagonal dapped-end reinforcement

L_{sH} horizontal dapped-end reinforcement length

Q applied load

V shear force at the dapped-end

V_y shear force at the dapped-end for the first reinforcement yielding

V_u shear strength of the dapped-end

$V_{u,avg}$ shear strength of the dapped-end (average between replicated tests)

1. Introduction

Dapped-end beams (DEB), also known as Gerber joints or half joints, are frequently used at supports in reinforced and prestressed concrete structures, particularly in precast concrete manufacturing. Their shape facilitates the connection of precast structural elements, enables expansion joints to be built and lowers the height of floors (see an example of application and typical geometry in Fig. 1(a)). Despite standard concrete details and extensive past experimental research [1–10], major durability issues, and even collapses, have been observed in DEB structures [11,12]. This explains the numerous studies performed lately on DEB [13–24], which focus mainly on strengthening measures, durability and the impact of deficient detailing. A detailed overview of the dimensions and characteristics of experimental tests on reinforced concrete DEB reported in the literature can be found elsewhere [12,22].

While some guidelines [25] propose specific empirical and semi-empirical design rules, DEB are typically designed by either the strut-and-tie method [26] or the stress fields method [27–30]. These mechanical approaches allow the dproper detailing of structural elements based on flow of forces (Fig. 1(a)), which makes them most suitable for regions with some source of discontinuity (static and/or geometric), such as DEB. Since both methods are grounded on the lower bound theorem of limit analysis, they are safe if enough deformation capacity is provided to simultaneously develop the plastic capacity of different strength mechanisms. Nevertheless, the accuracy of these methods strongly depends on the appropriate verification and location of concrete regions (nodal regions and struts), which is a major limitation when applied to DEB because of the complexity of the nodal region located on top of their hanger reinforcement (main vertical ties).

The nodal region on top of the hanger reinforcement in DEB is a restrictive case of compression-compression-tension (CCT). While the anchorage of the reinforcement in standard CCT nodes over supports is typically produced totally or partially outside the nodal region, the hanger reinforcement in DEB does not even cross the node entirely (Fig. 1(b)). A similar situation occurs in other structural elements, such as frame corners with opening moments [31]. So unless the concrete cover of these elements is neglected, the deviation of the compression flow of forces implies tensile stresses in the unreinforced cover, which may cause spalling failures (see Fig. 1(b)). While the distribution of reinforcement on several layers spreads these deviation forces by reducing, or even avoiding, spalling [31], the cover spalling phenomenon has often been observed [4,5] to be the governing failure mode of DEB with a concentrated hanger reinforcement. Cover spalling has been extensively studied for columns, especially for high- and ultra-high strength and steel fibre-reinforced concrete columns [32,33], but it is not easy to extrapolate the proposed models to DEB and they are unsuitable for design purposes. Therefore, DEB designers are unable to assess cover spalling, which hinders the geometric definition of strut-and-tie models because spalling significantly modifies the position of the horizontal upper strut and, therefore, the whole geometry of the strut-and-tie model to be considered in the region.

Verifying DEB with a concentrated hanger reinforcement may lead to non-conservative results when considering the strength of the CCT nodes included in standards, unless the contribution of the concrete cover is neglected, as previously recommended [4,5]. This simplification provides conservative results, especially as to whether the failure load is not limited by cover spalling and may be unsuitable to assess existing structures. Consequently, designers may find a few uncertainties when applying strut-and-tie models for DEB with a concentrated hanger reinforcement, namely: (i) the location of nodes when considering the cover spalling phenomenon; (ii) the influence of the location of stirrups in the vicinity of the corner and the stirrups on the beam; (iii) the reduction factor that accounts for the presence of transversal strains and concrete brittleness in the vicinity of the CCT node on top of the hanger reinforcement.

Therefore, this paper mainly aims to study the failure mode of dapped-end beams with different amounts and distributions of reinforcement by carrying out an experimental campaign of 28 tests, and by paying special attention to the spalling of the concrete cover. The campaign was designed to assess the influence of the following variables on the strength of DEB: amount of reinforcement, layout of vertical reinforcement, distribution of horizontal and vertical reinforcements, and presence of diagonal reinforcement.

As a result of this study, a simplified procedure to define the geometry of strut-and-tie models is provided, which accurately predicts the strength of 39 DEB tests taken from the literature and the new test presented herein. The new proposed approach allows designers to define the geometry of STM according to the orthogonal and diagonal reinforcements for elements with and without the spalling of the concrete cover on top of the hanger reinforcement for either verification or design purposes.

2. Test campaign

A description of 28 dapped-end tests, which belong to 15 beam specimens, is offered in the following sections. Further details of the complete experimental campaign can be found in [12].

2.1. Test specimens

Fig. 2 shows the geometry of the elements. The beam span was 3000 mm long, with a rectangular 250x600 mm cross-section, reduced to 250x300 mm on the nib. All 15 beam specimens were laid out with the same reinforcement on both dapped-ends. Each end was tested separately and, therefore, the test was replicated for all 15 analysed configurations.

Fig. 3 shows the nomenclature for each reinforcement. The dapped-end reinforcement variables comprised diagonal bars (sD), horizontal bars (sH) and vertical stirrups (sV), arranged on one ($sV1$) or three layers ($sV1$, $sV2$ and $sV3$). Beam reinforcement was composed of both flexural reinforcement ($sF1$ and $sF2$) and shear reinforcement (sT). The ends of the horizontal bars (sH) and the flexural beam reinforcement ($sF1$) were welded to steel plates of 250x100x10 mm^3 to ensure perfect anchorage conditions. The length of the horizontal bars was laid out for each amount of reinforcement so that anchorage would not limit the capacity of the support (850 mm, 1,000 mm and 1,250 mm, respectively, for the three different amounts presented below).

Table 1 contains the main properties of the specimens. Specimens DEB-1.1 to DEB-1.9 did not include diagonal reinforcement and were designed to study three layouts for orthogonal reinforcement with different ratio values of the horizontal reinforcement amount related to the hanger reinforcement amount (A_{sH}/A_{sV}). Layout O.1 (specimens DEB-1.1, DEB-1.4, DEB-1.6 and DEB-1.8) is the reference configuration, which was designed by means of a strut-and-tie model [12] according to EN 1992-1-1 [34] and neglecting the contribution of the concrete cover as proposed by Cook and Mitchel [4,5]. This model leads to an inclination of the strut from the support of 34º and consequently to a ratio A_{sH}/A_{sV}≈1.5. Layouts O.2 and O.3 analyse the effect of deficient detailing by under-reinforcing the horizontal and the hanger reinforcement of configuration O.1, respectively. In layout O.2 (specimens DEB-1.2, DEB-1.5, DEB-1.7 and DEB-9) the horizontal reinforcement was under-reinforced a 40%, leading to A_{sH}/A_{sV}≈0.9, while in layout O.3 (specimen DEB-1.3) the hanger reinforcement was under-reinforced a 60%, leading to A_{sH}/A_{sV}=3.9. Moreover, the effect of arranging sV on one layer or on three layers was studied for layouts O.1 and O.2.

Specimens DEB-2.1 to DEB-2.6 included diagonal reinforcement bars (sD) with an inclination (β_D) of 47º in addition to the orthogonal reinforcement. In layouts D.1, D.2 and D.3 the diagonal reinforcement was added to the reference orthogonal configuration (i.e. layout O.1). The amount of diagonal reinforcement was set based on a strut-and-tie model [12] so that the contribution at failure of the inclined mechanism to total specimen strength was approximately 40% for layout D.1, 60% for D.2 and 80% for D.3. Specimen DEB-2.6 laid out the layout of reinforcement D.4.1, which consisted in a variation of D.3 with a 5-fold increase in horizontal reinforcement. The horizontal length of the diagonal bars (L_{sD} in Fig. 3) was laid out for each amount of reinforcement (350 mm, 470 mm and 600 mm, respectively).

In both series, three different amounts of reinforcement were analysed, coded p100, p71 and p49, which indicate the percentage of reinforcement of each specimen in relation to that of the maximum reinforcement amount of its series. The diameter and/or number of bars were changed (see Table 1) to reach the targeted amounts of reinforcement.

2.2. Material properties

Specimens were cast in three batches with normal strength concrete and a maximum aggregate size of 20 mm. Compressive strength f_c was tested at the same age of each specimen by two 150x300 mm cylinder specimens. The averaged results are shown in Table 1. The scatter in the strength is caused mainly by strength differences between batches, with a limited influence of the testing age [12].

Conventional European reinforcing bars, with a nominal yield stress of 500 MPa and ductility grade B (according to EN 1992-1-1 [34]), were used in the specimens. The average mechanical reinforcement properties of two tests per diameter are presented in Table 2.

2.3. Test setup, instrumentation and test procedure

The test setup is presented in Fig. 2. The simply supported specimens were loaded under three-point non-symmetric bending, with a span (distance between the two support axes) of 2,500 mm. Load (Q) was applied to the centre of the beam by a 2.5 MN hydraulic actuator, arranged with a load cell on a reaction structure (Fig. 2) at 1,500 mm from the tested support. Hence the reaction (V) at the tested end was 40% of the applied load. After running the test of the first dapped-end, the setup was inverted to test the second end. Load was displacement-controlled at a rate of 0.25 mm/min.

Supports were composed of a system of PTFE (Teflon) and polished stainless steel 5-mm plates to allow rotations and horizontal sliding. Neoprene (250x150x20 mm) was placed over the sliding system to ensure a uniform reaction.

Up to 45 strain gauges per test were located on reinforcing bars (see the location for DEB-1.6 in Fig. 4) to the control strains and to determine the yield points. The strain measurements on the different instrumented bars of a certain section were averaged for further analyses. A photographic shoot system (1 Hz frequency) was run for imaging control purposes.

3. Tests results and discussion

All the specimens failed in the tested support, except for DEB-1.1 (T2), DEB-1.5(T2), DEB-2.3 (T2) and DEB-2.6 (T2), in which the concrete of the tested region was pre-damaged during the first test of the specimen (e.g. local concrete failure on the intermediate support). Hence these tests failed prematurely and their results were either completely (DEB-2.3 (T2) and DEB-2.6 (T2)) or partially (DEB-1.1 (T2) and DEB-1.5 (T2)) dismissed.

Table 3 shows the results of the reaction on the tested support at two singular points: first yielding (V_y) and peak load (V_u). Table 3 also contains for both singular points the strains of each dapped-end reinforcement (ε_{si}, where '*si*' follows the reinforcement notation of Fig. 3).

3.1. Mode of failure

Spalling of concrete cover

The tests showed cracking that ran in parallel to the diagonal compression field over the tested support, except for specimen DEB-1.3. This cracking progressed up to the top of the hanger reinforcement where a delamination crack subsequently developed at the top reinforcement level. The delamination crack always took place upon peak load; only in some tests did it become suddenly unstable immediately after the peak load had been reached, which led to fragile spalling failure (Fig. 5 shows this kind of fragile failure caused by the spalling of the top cover for test DEB-1.6 (T1)). This spalling behaviour agrees with previous observations made by Cook and Mitchell [4,5]. The crack patterns for four tests are shown in Fig. 7, in which the cracks in the diagonal corner at 30% of the peak load are highlighted in blue, while the main cracks for the peak and post-peak phases are highlighted in red.

Three criteria were applied to distinguish the tests with spalling failure: (i) a delamination crack was produced upon maximum load; (ii) no horizontal plateau was observed on the load-displacement curves before the peak load was reached; (iii) the post-peak strength dropped after the maximum load by more than 20% for a 20% increase in the deflection in the centre of the beam. With these criteria, neither those tests with spalling cracks that did not become unstable, nor those in which spalling failure took place in the post-peak phase, were classified as spalling delamination. Fig. 6 shows the graphical application of these criteria for specimens DEB-1.6 and DEB-1.7, in which the load-displacement curves are represented relative to the peak load and to the displacement at peak load. It can be observed that both tests of specimen DEB-1.6 showed a brittle behaviour after peak load (criteria III), without developing a plateau before reaching the peak-load (criteria II). Therefore, both DEB-1.6 tests are classified as spalling failures, while DEB-1.7 tests, which showed a ductile post-peak behaviour, not. Table 3 indicates for all tests when spalling failure was observed according to the proposed classification.

The behaviour of both tests (T1 and T2) of specimen DEB-1.3 was singular. Given the very small amount of hanger reinforcement in this specimen, a single crack developed after yielding this reinforcement from the edge of the support up to the top of the second shear stirrup of beam reinforcement (see Fig. 7(a)). Brittle crack sliding failure eventually took place once this crack suddenly propagated along the top of the shear reinforcement of the beam.

Yielding reinforcement steel

As shown in Table 3, some, or all, the ties yielded before the peak load was reached. The first yielding occurred between 47% and 78% of the ultimate load. Detailed results about the first yielding and the sequence of the yielding of the different reinforcements in the dapped-end region are provided in Table 3. Four different test groups can be distinguished for the yielding sequence:

- For the specimens with layout of reinforcement O.1, reinforcements *sV* and *sH* yielded at similar load levels (as was expected from the design of this reference layout, see section 2.1) for those cases in which the hanger reinforcement was placed on a single stirrup. For those cases in which the hanger reinforcement was distributed into three stirrups, the progressive yielding of these stirrups was observed, which started from the closest one to the support and with the horizontal reinforcement yielding always occurring before the last stirrup yielding. Upon peak load, *sH* and each stirrup of *sV* always yielded, as seen for DEB-1.6 (T2) in Fig. 8(a).
- For the specimens with layouts of reinforcement O.2 and O.3, yielding first took place at the lower reinforced tie in relation to configuration O.1. Large stress redistributions were observed after this initial yielding. Therefore, even the over-reinforced tie yielded for some tests according to these configurations. In configuration O.2, where the hanger reinforcement was distributed into three stirrups, the first stirrup always yielded and the last one always remained elastic; e.g., see DEB-1.7 (T2) (Fig. 8(b)).
- For those specimens to which diagonal reinforcement was added to reinforcement layout O.1 (specimens DEB-2.1 to DEB-2.5), the strains of the hanger reinforcement were similar to the strains of the horizontal

reinforcement, identically as observed without diagonal reinforcement. The ratio between the strains of these orthogonal ties (*sV* and *sH*) and the strains of *sD* before yielding increased when the inclined mechanism contributed to the specimen's total strength. In this way, the diagonal reinforcement (orientated approximately in the principal strain direction of the elastic solution) was the first to yield in all the specimens, except in DEB-2.5 with the biggest contribution of the inclined mechanism (larger than the theoretical contribution given by an elastic analysis, i.e. around 75%). The plastic redistribution capacity was large enough in all cases, and allowed the orthogonal and inclined mechanisms to develop their maximum capacity upon peak load, independently of which mechanism was first yielded.

- For specimen DEB-2.6 (similar to DEB-2.5, but with a much bigger amount of horizontal reinforcement), the orthogonal mechanism yielded before the diagonal one. Given its considerable over-strengthening, in this case the horizontal reinforcement remained elastic until failure.

3.2. Scatter between replicated tests

As stated in Section 2.1. , a total of two tests were done for each one of the 15 analysed reinforcement configurations (see results in Table 3). This gives a valuable information about the uncertainty of the measured strength capacity, caused by the scatter of the physical process itself (e.g. scatter of the material properties), as well as construction imperfections and testing errors. Fig. 9 represents the relative variation of the measured shear strength in each test respect to the average shear strength between replicated tests ($V_{u,avg}$). As a reference, the available tests in the literature containing replications [6,13,15] have been included as well into Fig. 9. The average deviation of individual tests to the average value of a certain reinforcement configuration is around 3% in this as well as in previous studies. While specimen 1.6 showed clearly the higher scatter of the experimental campaign, with a deviation of the two tests around 10% from the average value, it can be seen that the deviation was below 5% in most specimens.

3.3. Influence of the amount of reinforcement

Three different reinforcement layouts in this research (D.1, O.2 and O.1 with the hanger reinforcement distributed into three stirrups) were tested with exactly the same geometry for three different amounts of reinforcement. Independently of each configuration, Table 4 shows the average ultimate loads for each amount of reinforcement (V_u) in relation to the average ultimate loads of the smallest amount of reinforcement ($V_{u,\mathrm{p}49}$). In this analysis, the average strength results of the two tests for each specimen were used. An increase in reinforcement of 50% and 100% enhanced strength by around 15% and 60%, respectively, with very similar results for the three tested reinforcement layouts. Hence strength clearly increased less than the increase in reinforcement, which suggests that concrete failure should limit the ultimate load for the largest amounts of reinforcement. This is consistent with the observed spalling failure modes (less affected the specimens with the lowest reinforcement content). Thus it can be concluded that the spalling failure of the cover on top of the hanger reinforcement clearly limited the ultimate load of DEB, except for very small reinforcement amounts.

3.4. Influence of hanger reinforcement distribution

Hanger reinforcement was arranged on one stirrup or on three. This factor was analysed exclusively for the smallest amount of reinforcement by the following specimens: DEB-1.1 *vs.* DEB-1.4 and DEB-1.2 *vs.* DEB-1.5. It can be concluded from Table 3 that the distribution of the same amount of reinforcement on three stirrups reduced the strength by 10% on average. This reduction can be explained by the mechanical centre of the hanger reinforcement not remaining constant when increasing the number of stirrups: it was 17% further away from the support than in the configuration with one stirrup. While this increase in the shear span-to-depth ratio tended to reduce strength capacity almost proportionally, it was partially compensated by the positive effect on the spalling failure mode of the hanger reinforcement distribution (since the deviation of the compression field spread and, thus, the tensile stresses that generated on the cover reduced). For larger amounts of reinforcement and/or wider hanger reinforcement distributions, this positive effect could even compensate the increase in the shear span-to-depth ratio, which should be further investigated.

3.5. Influence of the A_{sH}/A_{sV} ratio

The layout of reinforcement O.2 consisted in a 40% reduction in A_{sH} in relation to reference layout O.1, which was tested for all three different amounts of analysed reinforcement. The layout of reinforcement O.3 (40% reduction in A_{sV} compared to layout O.1) was tested only for the smallest amount of reinforcement. Table 5 shows, similarly to Table 4 for the amount of reinforcement, the averaged ultimate loads for each layout of reinforcement in relation to the average ultimate loads of the reference layout O.1 ($V_{u,\mathrm{O.1}}$). The 40% reduction in A_{sH} in O.2 led to slightly lower reductions in strength (around 30%), with similar results regardless of the amount of reinforcement. This difference is related to the described layout O.2 behaviour, in which not all the stirrups of the hanger reinforcement reached their maximum capacity upon failure (see Fig. 8). According to this observation, the mechanical resultant of A_{sV} came closer to the edge, while the diagonal strut from the support was steeper than in layout O.1 and was, therefore, more efficient for a given horizontal capacity. For configuration O.3, the 60% reduction in A_{sH} in relation to the reference layout O.1 led to a much less marked reduction in strength (34%). This difference can be explained by the significant contribution of beam shear reinforcement (sT); the tests of specimen DEB-1.3 with layout O.3 developed a significant redistribution to this mechanism after yielding the hanger reinforcement.

3.6. Influence of the ratio between the orthogonal and inclined mechanisms

As previously described, the beams with inclined reinforcement showed a large enough plastic redistribution capacity to reach the maximum capacity of the orthogonal and inclined mechanisms for the different contributions of the analysed inclined mechanism. Therefore, the capacity of the dapped-end beams was given by the combination of the full capacity of the orthogonal and inclined mechanisms, regardless of the ratio between both mechanisms.

Besides strength capacity considerations, it should be note that the presence of inclined reinforcement improves the serviceability behaviour of dapped-end beams (as previously reported e.g. by Zhu et al. [9]), since it is oriented close to the principal tensile direction of the element. In this study, the inclined reinforcement reduced the crack openings at service loads between a 20% and a 40%, depending on the contribution of the inclined mechanism to total specimen strength. Further details of crack opening results for this experimental campaign can be found elsewhere [12].

4. Analysis with strut-and-tie models

4.1. Building strut-and-tie models from the experimental results

By means of strain gauges, the strains of the reinforcement bars were measured at their main sections close to the dapped-end (see the example in Fig. 4 for specimen DEB-1.6). The stresses and forces carried by the reinforcement were calculated based on the strain results by considering the nominal sections of the bars and assuming an idealised bilinear stress-strain relationship. The stress-strain relationship was defined for each reinforcement according to the measured mechanical properties (Table 2), and by considering a modulus of elasticity of 200 GPa and a strain at the maximum reinforcement stress of 5% (characteristic value required by EN-1992 EC-2 [34] for the used steel B500B). Fig. 8 shows the results of stresses (colour) and forces (thickness) at the reinforcement for two tests upon peak load.

For the purpose of building strut-and-tie models based on the experimental results, the calculated forces carried by the reinforcing bars were considered to be tie forces for those gauges placed in the proximity of cracks since stress-free cracks were assumed. This is the case of the gauges located in the vicinity of the re-entrant corner (reinforcement bars *sH*, *sV* and *sD*) because the starting position of the diagonal crack at the re-entrant corner was known beforehand and gauges were strategically placed assuming a crack inclination of 45º. For the strain gauges not located in the proximity of a crack, the tie force could differ from the force carried by the reinforcement (calculated according to the measured strains) because of the tension-stiffening effect. For building strut-and-tie purposes, tie forces were estimated in these cases by the equilibrium conditions from the known tie loads.

The results of the strut-and-tie models compatible with the results measured upon peak load were built and are shown in Fig. 10 for four different tests (struts are represented in dashed black lines with a thickness proportional to their resisted loads, and ties are denoted by thin continuous black lines superposed to the measured reinforcement loads). The detailed results of the forces in the struts and ties for these models are provided in Table 6. The hanger reinforcement was grouped into a single tie in DEB-1.6 (T2) and DEB-1.7 (T2) adding the measured forces in the three stirrups. Different models based on the experimental results could be built, but the basic morphology would remain the same. This allowed us to state the next qualitative analysis based on the particular models of Fig. 10:

- For configuration p100-O.1 (test DEB-1.6 (T2) in Fig. 10(a)), node 2 is located quite low, which is consistent with the observed spalling failure. Upon failure load, only tie 1-4 (reinforcement *sH*) yields, while the force of tie 2-3 (reinforcement *sV*) exceeds the magnitude of the reaction by 36% due to the vertical component of the fan stress field generated by the anchorage of the horizontal dapped-end reinforcement.
- Configuration p100-O.2 (test DEB-1.7 (T2) in Fig. 10(b)) has a lower ratio A_{sH}/A_{sV} than p100-O.1. The resulting strut-and-tie model of this configuration is similar to the previous one, but node 2 is located higher, which is consistent with the observed mode of failure without spalling. Upon peak load, tie 1-4 (reinforcement *sH*) yields, while the force of tie 2-3 (reinforcement *sV*) exceeds the magnitude of the reaction by only 17%.
- For configuration p49-O.3 (test DEB-1.3 (T1) in Fig. 10(c)), with a higher ratio A_{sH}/A_{sV} than p100-O.1 (test DEB-1.6 (T2)), both the hanger and the horizontal dapped-end reinforcement reach their capacity. As the magnitude of the reaction is greater upon failure than the capacity of the vertical reinforcement, the remaining vertical component of the reaction must be equilibrated by the contribution of the first stirrup of the beam.
- In configuration p100-D.1 (test DEB-2.2 (T1) in Fig. 10(d)), which contains diagonal reinforcement, all the main dapped-end reinforcements (*sD*, *sH* and *sV*) yield. Upon failure, the sum of the vertical component of the diagonal tie 1-5 capacity and the vertical tie 2-3 capacity equals the reaction. Since node 2 is lower than the compression chord of the beam, there must be two struts: strut 2-6 that connects the compression chord trajectory and strut 2-4 that represents the fan stress field generated by the anchorage of the horizontal dapped-end reinforcement.

4.2. Simplified strut-and-tie models for dapped-end beams

Based on previous observations, it can be stated that the failure of the nodal region on top of the hanger reinforcement strongly impacts the geometry of the strut-and-tie models for dapped-end beams. Some authors have suggested neglecting the contribution of the top concrete cover when computing this nodal region [4,5]. While this is a simple safe approach, it can be excessively conservative for assessment, and even design purposes. The verifications proposed by standards to check compression-compression-tension (CCT) nodal regions could be potentially unsafe [4,5] when applied to dapped-end beams if the contribution of the concrete cover is considered; these verifications are derived for the CCT nodes over supports, but dapped-end beams have more restrictive conditions: (i) the reinforcement in the node is typically yielded in the ultimate state and (ii) part of the nodal region is unreinforced since reinforcement does not completely cross it (and not as in the CCT nodes over supports). A refined analysis of the behaviour of this nodal region would be time-consuming and require knowing variables such as concrete tensile strength and exact reinforcement detailing. For this reason, the development of simplified procedures, which allow a simpler, yet accurate, calculation of the load capacity of dapped-end beams without neglecting the top concrete cover, is most relevant. The simplified procedure now presented is derived for (i) reinforced dapped-end beams, (ii) with a clearly defined hanger reinforcement and (iii) without any other reinforcement on the support apart from the main reinforcements defined in Fig. 11. The additional detailing reinforcement used to control tensile stresses due to the diffusion of the strut on the support required for dapped-ends with profound depths does not need to be considered in a global strut-and-tie. Hence in those cases which would require this reinforcement, the simplified proposed procedure is still applicable.

4.2.1. Model description

Based on the experimental observations discussed in Section 4.1. the model considers that (i) concrete does not fail out of the nodal region on top of the hanger and (ii) the diagonal and horizontal reinforcement in DEB always develops its plastic capacity. Two different strut-and-tie models may produce upon failure, depending on whether the hanger reinforcement yields or not:

- Model A (Fig. 11(c)), if the hanger reinforcement does not reach its maximum capacity. In this case, the vertical reaction (V) of the support is equilibrated by (i) the vertical component of the diagonal reinforcement whenever present and (ii) the hanger reinforcement. In this model, the hanger reinforcement also supports the action of the fan anchorage mechanism of the horizontal reinforcement (strut 4 in Fig. 11(a)).
- Model B (Fig. 11(e), when the hanger reinforcement reaches its plastic capacity. In this model the vertical reaction is equilibrated by three resistant mechanisms: (i) the vertical component of the diagonal reinforcement whenever present; (ii) the hanger reinforcement; (iii) the contribution of beam shear stirrups. In this case, no fan anchorage mechanism for the horizontal reinforcement is produced and all the hanger reinforcement capacity equilibrates the load at the support.

If the position and strength of the different ties are known (Fig. 11(a)), the capacity of the proposed strut-and-tie models is dependent only on the vertical position of node 2 on top of the hanger reinforcement. The failure condition of this nodal region is required to obtain the maximum strength of the element. The simplified geometry shown in Fig. 11(b) is considered for this nodal area, which implies that the compression chord is stressed below its plastic capacity and does not limit the strength of the element. In order to easily define the vertical position of this nodal region upon failure, it is assumed that the failure condition of strut 1B-2 (see Fig. 11(b)) in node 2 provides a good estimation of this position, without being necessary to explicitly verify the nodal area.

Based on the experimental observations, the model assumes that the capacity of the diagonal strut can be expressed by a unique expression with a reduction factor (k_c) that takes into account cover spalling and the presence of transversal strains regardless of the element's mode of failure (with or without spalling). In this way, the maximum compressive load of strut 1B-2 (see Fig. 11(b)) can be expressed as follows:

$$C_{1B-2} = k_c \cdot f_c \cdot b \cdot \left(2 \cdot x \cdot \cos\theta_{1B-2}\right) \tag{1}$$

where b is the width of the dapped-end beam, x is the vertical distance between node 2 and the top edge of the beam, and θ_{1B-2} is the inclination of strut 1B-2.

Verification approach – Model A

By applying this failure criteria for the proposed model A and considering the horizontal equilibrium at node 1A, as well as the equilibrium at node 1B (described at Fig. 11(d)), it is possible to obtain the vertical position of node 2 according to the geometry, concrete strength and the capacity of ties. This result can be expressed as the slope between nodes 1A and 2 as follows:

$$\frac{z}{a_V} = \lambda_d - \lambda_c + \sqrt{\lambda_c^2 + 2 \cdot \lambda_c \cdot \left(\frac{d}{a_1} - \lambda_d\right) - 1} \tag{2}$$

where z is the vertical distance between node 2 and the horizontal dapped-end reinforcement, a_V is the horizontal separation of the hanger reinforcement to the strut-and-tie node over the support (1A), d is the effective depth in the nib, and λ_c and λ_d are dimensionless coefficients related to the capacity of the diagonal reinforcement and of concrete, respectively, both of which are normalised by the element's horizontal capacity:

$$\begin{aligned} \lambda_c &= \frac{k_c \cdot f_c \cdot b \cdot a_V}{T_{sH,u} + T_{sD,u} \cdot \cos\beta_D - H} \\ \lambda_d &= \frac{a_D}{a_V} \cdot \frac{T_{sD,u} \cdot \sin\beta_D}{T_{sH,u} + T_{sD,u} \cdot \cos\beta_D - H} \end{aligned} \tag{3}$$

where a_D is the horizontal separation of the diagonal dapped-end tie to the strut-and-tie node over the support (1A), $T_{sH,u}$ and $T_{sD,u}$ are the plastic tensile capacities of the horizontal and the diagonal dapped-end reinforcement, respectively, and H is the horizontal force applied at the dapped-end.

The ultimate load of the element (V_u) in model A can be derived from the moment equilibrium of the forces that act on the solid represented in Fig. 11(c) at node 2, which lead to Eq. (4). Thus the forces of struts C_3 and C_4 and the force of the vertical main tie (T_{sV}) are not required to compute the ultimate load.

$$V_u = \left(T_{sH,u} + T_{sD,u} \cdot \cos\beta_D - H\right) \cdot \frac{z}{a_V} + T_{sD,u} \cdot \sin\beta_D \cdot \left(1 - \frac{a_D}{a_V}\right) \tag{4}$$

This formulation is only valid for model A, which requires the hanger reinforcement to not reach its plastic capacity. To assess this condition, the contribution of hanger reinforcement (T_{sV}) can be derived by checking the vertical equilibrium of the element, which results in the following expression:

$$T_{sV} = \left(T_{sH,u} + T_{sD,u} \cdot \cos\beta_D - H\right) \cdot \tan\theta_{1\text{B-}2} + \mathrm{C}_4 \cdot \sin\theta_4 \tag{5}$$

where θ_4 is the slope of strut 4 and $\theta_{1\text{B-}2}$ is the slope of strut 1B-2, which is related to the geometry previously defined in Eqs. (2) and (3) as follows:

$$\tan\theta_{1\text{B-}2} = \frac{z}{a_V} - \lambda_d \tag{6}$$

Eq. (6) results in tan $\theta_{1\text{A-}2}$ for those cases with no diagonal reinforcement because a single direct strut forms between nodes 1A and 2.

Strut C_4 is produced by the action of the fan anchorage mechanism of the horizontal reinforcement, but only if the hanger reinforcement has enough capacity to equilibrate its vertical component (i.e. strut C_4 uses the remaining capacity of the hanger reinforcement after equilibrating the vertical component of strut 1B-2). Hence C_4 vanishes during the transition between model A and B. Thus model A is produced when the following condition is fulfilled:

$$\left(T_{sH,u} + T_{sD,u} \cdot \cos\beta_D - H\right) \cdot \tan\theta_{1\text{B-}2} \leq T_{sV,u} \tag{7}$$

Verification approach – Model B

When the condition given by Eq. (7) is not fulfilled, the ultimate load of the element (V_u) is given by model B, which considers the contribution of the beam shear reinforcement as follows:

$$V_u = T_{sV,u} + T_{sD,u} \cdot \sin\beta_D + T_{sT} \tag{8}$$

where the contribution of the beam shear reinforcement in model B (T_{sT}) is obtained from the equilibrium of the horizontal forces at node 1A and can be computed as follows:

$$T_{s3} = \frac{z}{a_3}\left(T_{sH,u} + T_{sD,u} \cdot \cos\beta_D - T_{sV,u} \cdot \cot\theta_{1\text{B-}2} - H\right) \leq T_{sT,u} \tag{9}$$

where z can be extracted from Eqs. (2) and (3) that define the vertical position of node 2, $T_{sT,u}$ is the plastic tensile capacity of the tie representing the shear reinforcement (*sT*) and a_3 is the horizontal separation of the beam shear tie to the strut-and-tie node over the support (1A).

In this model, the position of node 2 is assumed to be the same as for model A. While this is a conservative simplification for model B that users could overcome – by iteratively refining the position of node 2 in model B with the proposed formulation based on the load distribution between the two mechanisms (strut 1A-1B-2 *vs.* strut 1A-6) – no differences in the results were observed later between models A and B when using this simplification. Therefore, it is recommended to skip this refinement and apply the model without an iteration process.

Furthermore, if the shear reinforcement reaches its maximum capacity due to direct action from the support, the horizontal tie is not yield and its force can be obtained by:

$$T_{sH} = \frac{a_3}{z} T_{sT,u} - T_{sD,u} \cdot \cos\beta_D + T_{sV,u} \cdot \cot\theta_{1B\text{-}2} + H \tag{10}$$

For usual dapped-end designs, the vertical and/or diagonal reinforcements carry out the main part of the reaction, and the contribution of the beam shear reinforcement is minor. As indicated in Fig. 11(a), the consideration of all the shear stirrups that allow a direct strut with an inclination of at least 20º in the model is suggested.

Design approach

For design purposes, it is recommended to not rely on the contribution of the beam shear reinforcement and to use model A described above. Designers should first select the fraction of the vertical reaction to be equilibrated by the diagonal mechanism (α_D). Then the required capacities of the dapped-end ties can be expressed according to the acting vertical (V) and horizontal loads (H), as follows:

$$\begin{aligned}
T_{sH,u} &= V\left(1-\alpha_D\right)\frac{a_V}{z} + H \\
T_{sV,u} &= V\left(1-\lambda_d \frac{a_V}{z}\right) \\
T_{sD,u} &= \frac{V \cdot \alpha_D}{\cos\beta_D \cdot \frac{z}{a_V} + \sin\beta_D \left(1-\frac{a_D}{a_V}\right)}
\end{aligned} \tag{11}$$

where the z/a_V ratio that defines the vertical position of node 2 can be calculated for design purposes by the following expression:

$$\frac{z}{a_D} = \frac{1+\mu_c\lambda_d + \sqrt{1-2\mu_c\left(\frac{a_V}{d}-\lambda_d+\frac{a_V}{d}\lambda_d^2\right)-\mu_c^2\left(1+\lambda_d^2\right)}}{\mu_c + 2\frac{a_D}{d}} \quad (12)$$

in which λ_d was defined in Eq. (3) and μ_c is the following dimensionless coefficient:

$$\mu_c = \frac{V}{k_c f_c \cdot b \cdot d} \quad (13)$$

For those cases that include diagonal reinforcement, the proposed formulation requires an iterative resolution because λ_d coefficient is not known beforehand as it is dependent on the capacity of reinforcement (see Eq. (3)). When only orthogonal reinforcement is arranged, the λ_d coefficient is zero and the design process does not require any iteration. It should be noted that in spite of requiring an iterative solution for members with diagonal reinforcement, the proposed method allows for designing dapped-end beams easier than with conventional strut-and-tie modelling, for which the model's geometry has to be iteratively found depending on the verification of the CCT nodal area on top of the hanger reinforcement.

The proposed verification and design models only predict the strength of the dapped-end beams that reach their capacity due to reinforcement steel yielding and concrete failing on top of the hanger reinforcement. Hence additional verifications like stresses in other nodal regions and the appropriate anchorage of reinforcement have to be independently checked.

In the following section, the results of the verification model are compared to the experimental results for the different values of reduction factor k_c (that defines the effective concrete strength in the analysed strut, in Eqs. (1) and (3)) given in different design codes.

4.2.2. Comparison with the experimental results

Thirty-nine tests taken from Ajina [3], Clark and Thorogood [6], Zhu et al. [9] and Herzinger [13], as well as 28 of the tests presented herein, were used for the experimental verification of the proposed simplified strut-and-tie method for dapped-end beams. The analysis did not consider the second test for specimens DEB-1.1, DEB-1.5, DEB-2.3 and DEB-2.6, whose results were ruled out in ULS. Nor did the analysis consider the tests of the reference experimental campaigns [3,6,9,13], which contained factors that were not covered by the model, namely: (i) prestressing; (ii) T-sections; (iii) high-strength concrete; (iv) fibre-reinforced concrete; (v) other reinforcements on the support apart from *sH*, *sV* and *sD;* (vi) the distribution of the hanger reinforcement over many layers. The tests of Herzinger [13], which included an inclined reaction in DEB, allowed the verification of the proposed model for those cases with a horizontal component of the reaction.

To verify the compression-compression-tension (CCT) nodes, standards typically propose checking the strength of the diagonal strut. *fib* Model Code 2010 [35], EN 1992-1-1 [34] and ACI 318-14 [36] specify similar values for the strength of this diagonal strut, which lies at between 0.78- and 0.63-fold the uniaxial compressive strength depending on the compressive characteristic strength (see Table 7). For low concrete strengths, according to ACI 318-14 [36] the reduction factor is significantly lower than for the other two standards because the concrete brittleness reduction factor is set at 0.85, independently of compressive strength. These strengths, derived for CCT nodes on supports, would be unsafe for dapped-end beams, unless the top concrete cover is neglected. When considering the compressed cover, it is necessary to take into account the effect of the potential cracks crossing part of the diagonal strut, which can lead to delamination cracks, as previously described. Hence for this particular CCT node, the strengths given in the standards for struts with oblique tension might be more suitable. The compressive strength reduction factor for this strut case varies between 0.55 and 0.46 depending on the concrete strength (see Table 7) for the analysed standards [34–36], at around 30% lower than the values considered for the CCT nodes on supports.

The proposed verification model in Section 4.2.1. was applied to predict the ultimate load of the experimental tests selected for the two stated possible effective compressive strengths (standard CCT node or struts with oblique tension) according to *fib* Model Code 2010 [35]. Table 8 summarises the main results. The model barely depended on the effective concrete strength for the analysed range of strengths. Since the coefficients of variation for the ratio between the experimental and predicted loads were constant for the analysed cases, the strength reduction factor, given by *fib* Model Code 2010 [35] ($k_c=\eta_{fc}\cdot 0.55$), is recommended based on the analysis of the ratio between the experimental and predicted load and the percentage of unsafe predictions.

Fig. 12 graphically represents the predictions of the proposed model for this recommended factor. Details on the reinforcement capacity, geometry and mode of the proposed strut-and-tie model, and the predicted failure loads, for each analysed specimen are found in Table 9. While predictions were slightly conservative for the tests run by Zhu et al. [9] with very small amounts of reinforcement, for the reinforcement amounts used typically in the design practice, the model yielded accurate ultimate load estimations regardless of the reaction applied in DEB being vertical or inclined. The potential underestimation of capacity for lightly reinforced DEB could be due to (i) a significant contribution of concrete in tension for low reinforcement ratios and/or (ii) the dependence of the spalling process on the reinforcement ratio not being totally captured by the proposed model. While such amounts of reinforcement are below standard design practice, further experimental work on such elements would clarify these hypotheses and allow the proposed simplified model to be refined.

5. Conclusions

This paper presents experimental research about 28 tests of 15 different reinforcement configurations both with and without diagonal reinforcement. The elements' concrete strength and geometry were constant, while the amount and the layout of reinforcement were investigated. Hanger reinforcement either concentrated on a single layer or was distributed over a short distance (the same order as the concrete cover). Detailed measurements in the region near the support were recorded during the experimental tests. Based on the experimental results, a simplified procedure to define the geometry of the strut-and-tie models for DEB with concentrated hanger reinforcement is presented. The main research conclusions are:

- The deformation capacity of the tested DEB configurations is enough to develop the full strength of the orthogonal and inclined mechanisms, regardless of the ratio between mechanisms.
- The failure of the nodal region on top of the hanger reinforcement caused by concrete spalling limits the ultimate load of DEB, except for very low reinforcement ratios. This previously stated observation is confirmed by the experimental evidence provided herein for concentrated or quasi-concentrated hanger reinforcements.
- The verifications contained in the standards for CCT nodal regions are typically derived for the nodes on top of supports, and could lead to unsafe results when applied to the CCT nodal region of DEB on top of the hanger reinforcement, unless reinforcement is distributed or the top concrete cover is neglected. This CCT node in DEB is more restrictive than the standard CCT node since reinforcement is typically yielded in the node in the ultimate state and part of the nodal region is unreinforced.
- The simplified procedure presented herein, based on the strength of the diagonal strut from the support, allows the strength of the CCT node of DEB with concentrated reinforcement to be verified without neglecting the concrete cover from the geometry. Suitable results are obtained for the 65 analysed tests by considering the strength given in the standards for struts with oblique tension for this strut.
- The hanger reinforcement distribution over several layers reduces strength because of the resulting increase in the span-to-depth ratio, but this reduction is partially compensated by the positive effect on spalling failure. Further research is needed to analyse this positive effect, especially for large amounts of reinforcement, for which the procedure presented herein could be conservative when considering the reinforcement concentrated on a single layer.

Acknowledgements

The authors wish to thank the Spanish Ministry of Science and Innovation for funding Project BIA2009-11369 and for FPI fellowship BES-2010-030353 received by the first author. This work forms part of the first author's doctoral research awarded by the Business Chair of Sustainable and Advanced Construction at the Universitat Politècnica de València.

References

[1] Reynolds GC. The strength of half-joints in reinforced concrete beams.TRA415. London, UK: Cement and Concrete Association; 1969. p. 7.

[2] Mattock AH, Theryo TS. Strength of precast prestressed concrete members with dapped ends. PCI Journal 1986;34:58–75.

[3] Ajina JM. Effect of steel fibers on precast dapped-end beam connections. MSc Thesis. South Dakota State University, Brookings, South Dakota, EEUU; 1986. p. 271.

[4] Cook WD, Studies of disturbed region near discontinuities in reinforced concrete members. PhD Thesis. Structural Engineering Research Report 87-3, McGill University, Montreal, Québec, Canada; 1987. p 153.

[5] Cook WD, Mitchell D. Studies of disturbed regions near discontinuities in reinforced concrete members. ACI Structural Journal 1988;85:206–16.

[6] Clark LA, Thorogood P. Serviceability behaviour of reinforced concrete half joints. Structural Engineer 1988;66:295–302.

[7] Nanni A, Huang P-C. Validation of an alternative reinforcing detail for the dapped ends of prestressed double tees. PCI Journal 2002;47:38–49.

[8] Lin IJ, Hwang SJ, Lu WY, Tsai JT. Shear strength of reinforced concrete dapped-end beams. Structural Engineering and Mechanics 2003;16:275–294. doi:http://dx.doi.org/10.12989/sem.2003.16.3.275.

[9] Zhu RRH, Wanichakorn W, Hsu TTC, Vogel J. Crack width prediction using compatibility-aided strut-and-tie model. ACI Structural Journal 2003;100:413–421.

[10] Wang Q, Guo Z, Hoogenboom PC. Experimental investigation on the shear capacity of RC dapped end beams and design recommendations. Structural Engineering and Mechanics 2005;21:221–35. doi:http://dx.doi.org/10.12989/sem.2005.21.2.221.

[11] Johnson PM, Couture A, Nicolet R. Report of the Commission of inquiry into the collapse of a portion of the de la Concorde overpass. Québec, Canada; 2007. p. 198.

[12] Mata-Falcón J. Serviceability and ultimate behaviour of dapped-end beams (In Spanish: Estudio del comportamiento en servicio y rotura de los apoyos a media madera). PhD thesis. Universitat Politècnica de València, Spain; 2015. p. 719.

[13] Herzinger R. Stud reinforcement in dapped ends of concrete beams. PhD Thesis. University of Calgary, Calgary, Alberta, Canada; 2008. p. 324.

[14] Mitchell D, Cook WD, Peng T. Further examples for the design of structural concrete with Strut-and-Tie models - Example 14: Importance of reinforcement detailing. American Concrete Institute, ACI Special Publication 273, 2010, p. 237–51.
[15] Nagrodzka-Godycka K, Piotrkowski P. Experimental study of dapped-end beams subjected to inclined load. ACI Structural Journal 2012;109:11–20.
[16] Nagy-György T, Sas G, Dâescu AC, Barros JAO, Stoian V. Experimental and numerical assessment of the effectiveness of FRP-based strengthening configurations for dapped-end RC beams. Engineering Structures 2012;44:291–303.
[17] Lu W-Y, Lin I-J, Yu H-W. Behaviour of reinforced concrete dapped-end beams. Magazine of Concrete Research 2012;64:793–805.
[18] Moreno-Martínez JY, Meli R. Experimental study on the structural behavior of concrete dapped-end beams. Engineering Structures 2014;75:152–63.
[19] Atta A, Taman M. Innovative method for strengthening dapped-end beams using an external prestressing technique. Materials and Structures 2016;49:3005–19.
[20] Oviedo R, Gutiérrez S, Santa María H. Experimental evaluation of optimized strut-and-tie models for a dapped beam. Structural Concrete 2016;17:469–80.
[21] Aswin M, Mohammed BS, Liew MS, Syed ZI. Shear Failure of RC Dapped-End Beams. Advances in Materials Science and Engineering 2015:11.
[22] Desnerck P, Lees JM, Morley CT. Impact of the reinforcement layout on the load capacity of reinforced concrete half-joints. Engineering Structures 2016;127:227–39.
[23] Desnerck P, Lees JM, Morley CT. The effect of local reinforcing bar reductions and anchorage zone cracking on the load capacity of RC half-joints. Engineering Structures 2017;152:865–77.
[24] Desnerck P, Lees JM, Morley CT. Strut-and-tie models for deteriorated reinforced concrete half-joints. Engineering Structures 2018;161:41–54.
[25] Precast/Prestressed Concrete Institute. PCI design handbook 7th ed. Chicago, Illinois, USA; 2010. p. 828.
[26] Schlaich J, Schäfer K, Jennewein M. Toward a consistent design of structural concrete. PCI Journal 1987;32:74–150.
[27] Thürlimann B, Marti P, Pralong J, Ritz P, Zimmerli B. Application of the Theory of Plasticity to Structural Concrete (In German: Anwendung der Plastizitätstheorie auf Stahlbeton). Unterlagen zum Fortbildungskurs, Institut für Baustatik und Konstruktion, ETH Zürich, Switzerland; 1983. p. 252.
[28] Marti P. Truss models in detailing. Concrete International 1985;7:66–73.

[29] Nielsen MP, Hoang LC. Limit analysis and concrete plasticity. 3rd edition. Boca Raton, FL, USA: CRC press; 2010. p. 796.

[30] Muttoni A, Schwartz J, Thürlimann B. Design of concrete structures with stress fields. Basel-Boston-Berlin, Switzerland: Birkhaüser / Springer; 1997. p. 143.

[31] Campana S, Fernández Ruiz M, Muttoni A. Behaviour of nodal regions of reinforced concrete frames subjected to opening moments and proposals for their reinforcement. Engineering Structures 2013;51:200–10.

[32] Cusson D, Paultre P. High-strength concrete columns confined by rectangular ties. Journal of Structural Engineering 1994;120:783–804.

[33] Foster SJ. On Behavior of High-Strength Concrete Columns: Cover Spalling, Steel Fibers, and Ductility. ACI Structural Journal 2001;98:583–9.

[34] CEN European Committee for Standardization. Eurocode 2. Design of Concrete Structures Part 1-1: General Rules and Rules for Buildings. EN 1992-1-1, Brussels, Belgium; 2004. p. 225.

[35] Fédération Internationale du Béton (fib). *fib* Model Code for Concrete Structures 2010. Berlin, Germany: Wilhelm Ernst & Sohn; 2013. p. 402.

[36] American Concrete Institute Commitee 318. ACI 318-14 Building Code Requirements for Structural Concrete and Commentary, Farmington Hills, Michigan, USA: ACI; 2014; p. 519.

Table captions

Table 1. Properties of test specimens.

Table 2. Mechanical properties of reinforcement.

Table 3. Main results and failure modes of the experimental research.

Table 4. Influence of the amount of reinforcement on strength.

Table 5. Influence of the ratio between the horizontal and hanger reinforcement on strength.

Table 6. Forces in the strut-and-tie models proposed in Fig. 10 from the experimental results (F_h and F_v denote the horizontal and the vertical component of the force, respectively; negative force represents tension).

Table 7. Reduction factor of the compressive strength specified in *fib* Model Code 2010 [35], EN 1992-1-1 [34] and ACI 318-14 [36] for CCT nodes with anchorage outside the nodal region and struts with oblique tension.

Table 8. Statistical comparison of the test results to the proposed model for different effective compressive strength values (ratio V_{test}/V_{model}).

Table 9. Detailed results of the proposed model and a comparison to test the results (k_c=0.55·η_{fc}).

Figure captions

Fig. 1. Dapped-end beams: (a) typical geometry with strut-and-tie model for orthogonal reinforcement and (b) detail of the nodal area on top of the hanger reinforcement.

Fig. 2. Test setup for 3-point bending experiments on reinforced concrete dapped-end beams (dimensions in mm).

Fig. 3. Reinforcement notation and geometry (main reinforcement of the dapped-end in light grey; dimensions in mm).

Fig. 4. Strain gauges distribution on reinforcing bars (specimen DEB-1.6).

Fig. 5. Failure of test DEB-1.6 (T1): (a) view upon peak load and (b) view right after peak load.

Fig. 6. Example of application of spalling failure criteria for specimens DEB-1.6 and DEB-1.7.

Fig. 7. Crack pattern for the peak load represented in the photos taken after peak load (in blue highlighted cracking at 30% V_u).

Fig. 8. Reinforcement stresses (in colour, relative to the reinforcement yield strength f_y) and tensile forces (thickness) calculated from the strain measurements at peak loads: (a) DEB-1.6 (T2) and (b) DEB-1.7 (T2).

Fig. 9. Scatter between replicated tests (in the vertical axis the relative variation of the measured shear strength in each test respect to the average shear strength between replicated tests).

Fig. 10. Strut-and-tie models from the experimental results (struts represented in dashed black lines with a thickness proportional to their loads and ties in thin continuous black lines superposed to the reinforcement experimental results – represented by colour lines and text display of the measured force of each reinforcement layer –).

Fig. 11. Proposed simplified strut-and-tie models for dapped-end beams: (a) definition of ties; (b) node on top of the hanger reinforcement and verification section; (c)-(d) model A, description and equilibrium in nodes and (e) model B.

Fig. 12. Ratio between the experimental load and the load predicted by the proposed model (k_c=0.55·η_{fc}) versus the experimental load.

FIGURES

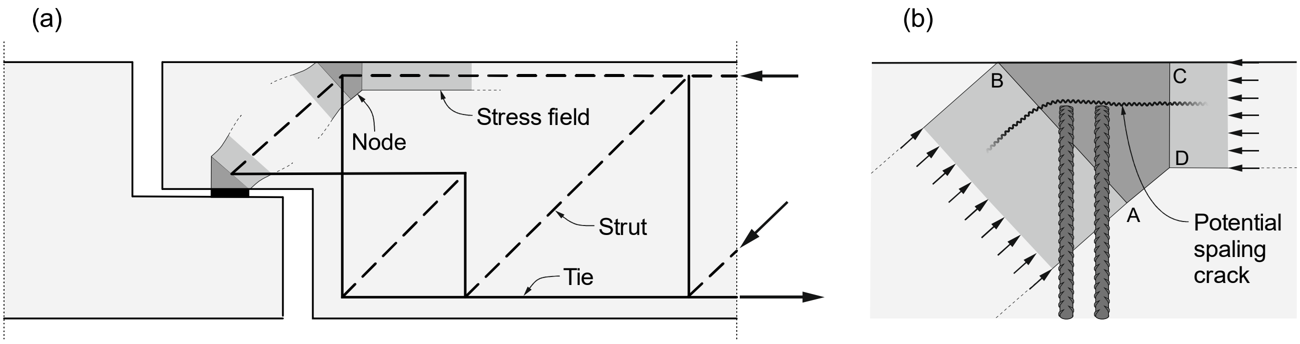

Fig. 1. Dapped-end beams: (a) typical geometry with strut-and-tie model for orthogonal reinforcement and (b) detail of the nodal area on top of the hanger reinforcement.

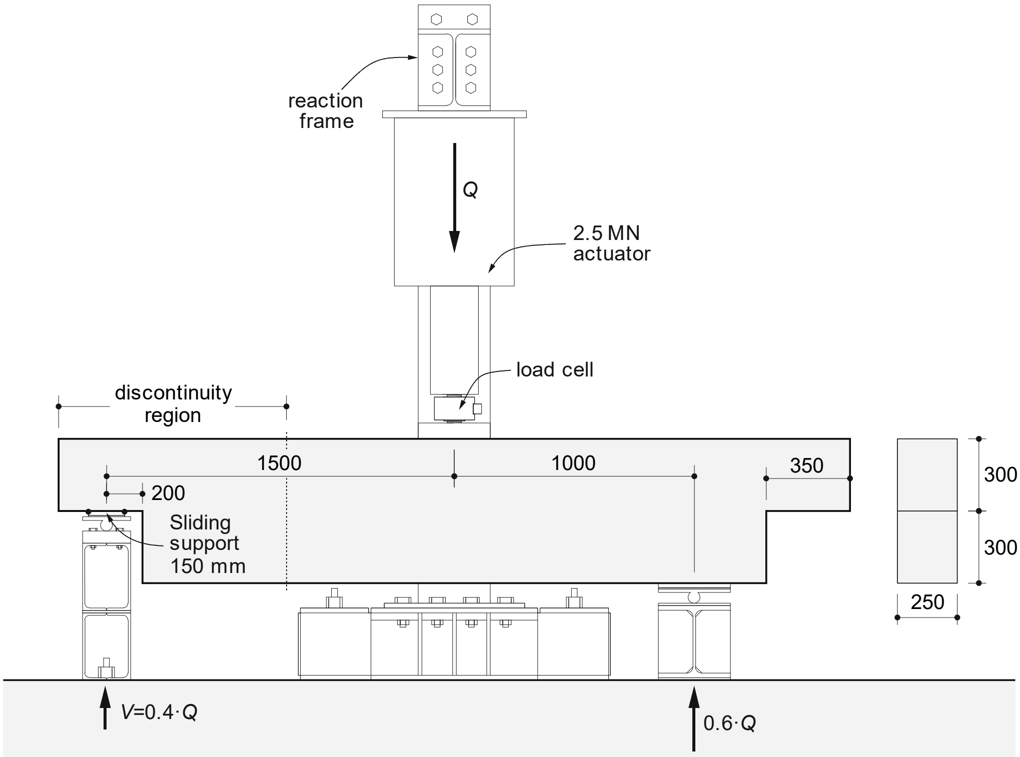

Fig. 2. Test setup for 3-point bending experiments on reinforced concrete dapped-end beams (dimensions in mm).

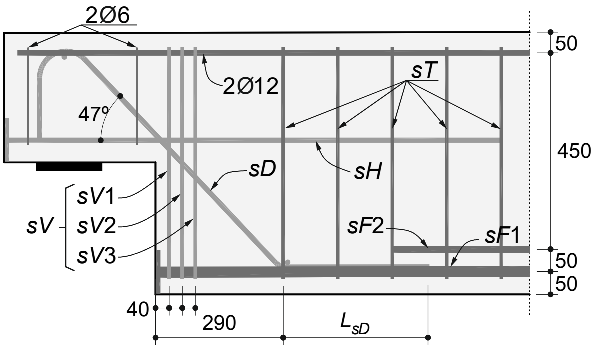

Fig. 3. Reinforcement notation and geometry (main reinforcement of the dapped-end in light grey; dimensions in mm).

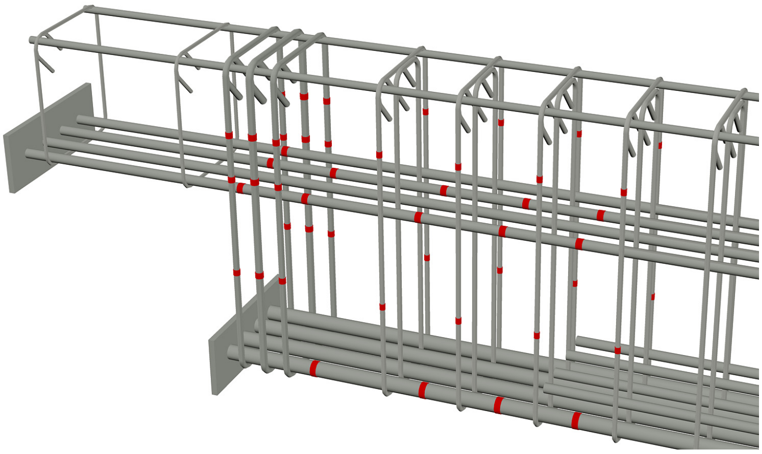

Fig. 4. Strain gauges distribution on reinforcing bars (specimen DEB-1.6).

(a) (b)

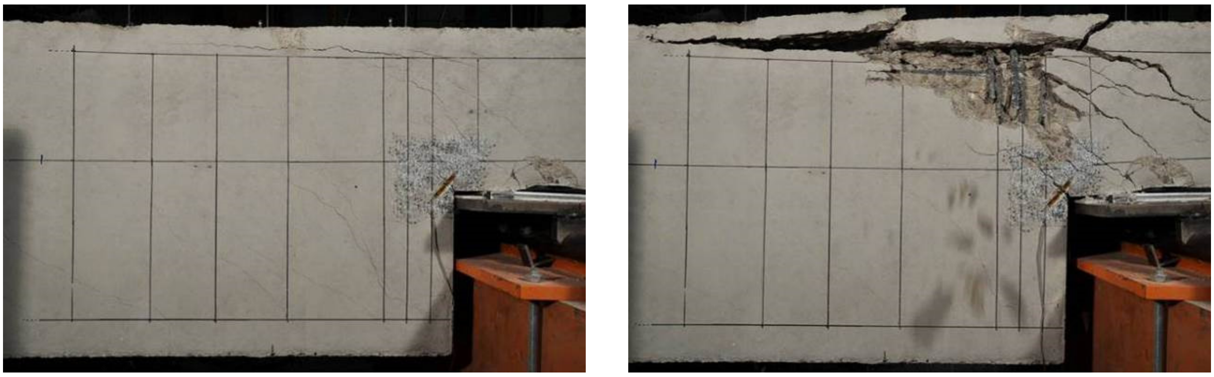

Fig. 5. Failure of test DEB-1.6 (T1): (a) view at peak load and (b) view one second after peak load.

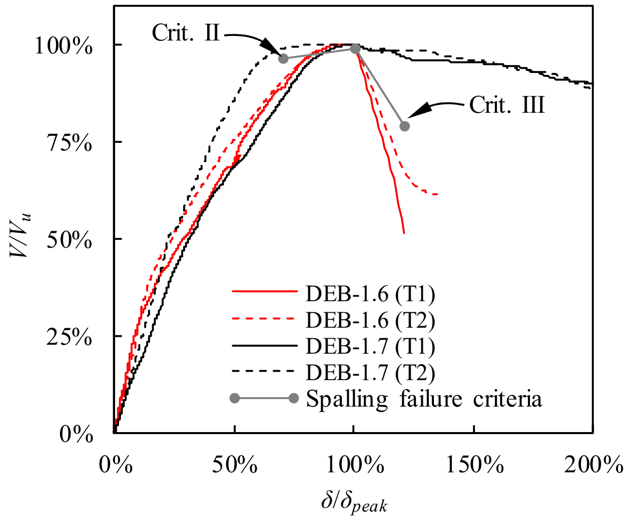

Fig. 6. Example of application of spalling failure criteria for specimens DEB-1.6 and DEB-1.7.

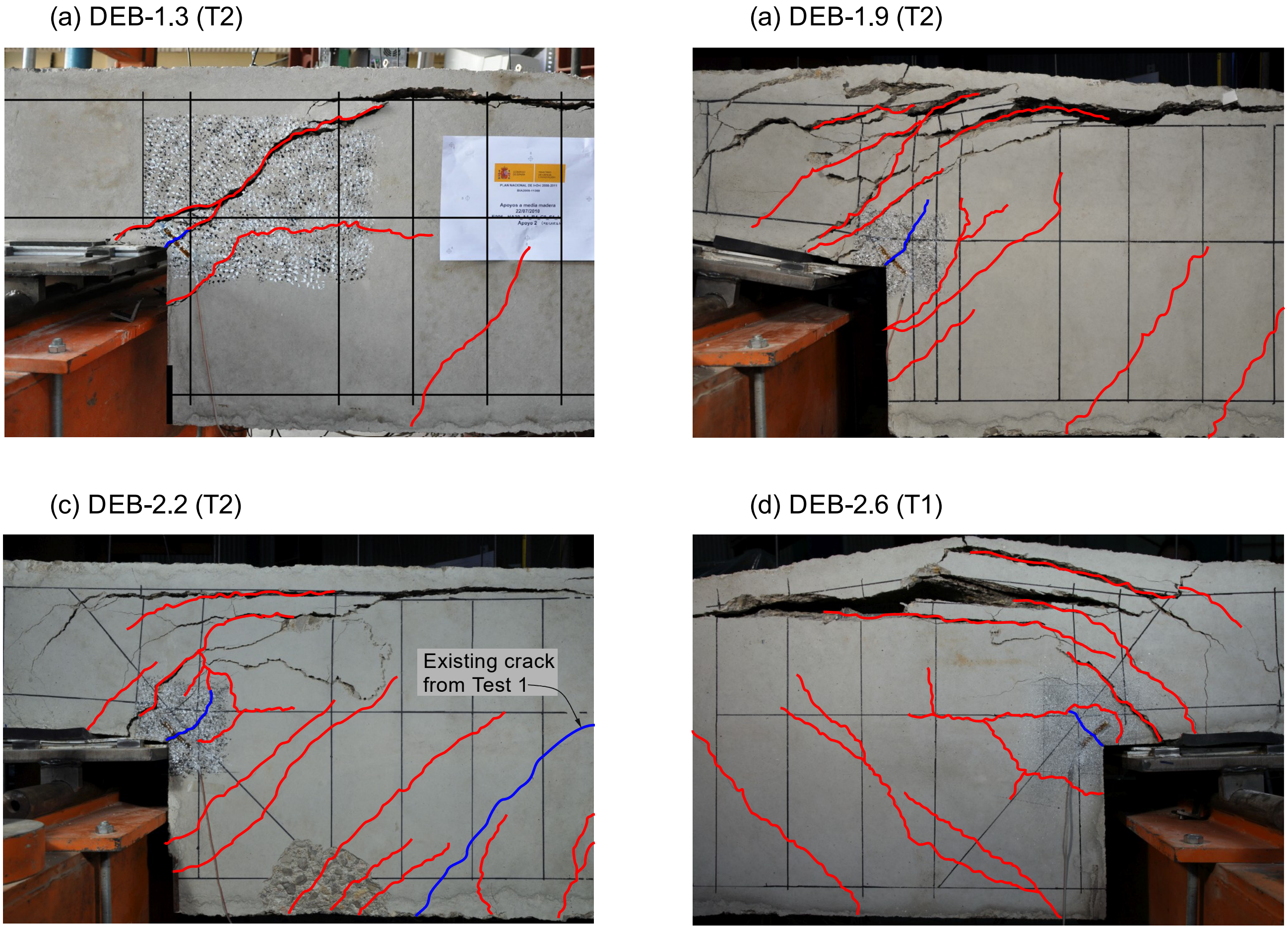

Fig. 7. Crack pattern for peak load represented in photos taken after peak load (in blue highlighted cracks at 30% V_u).

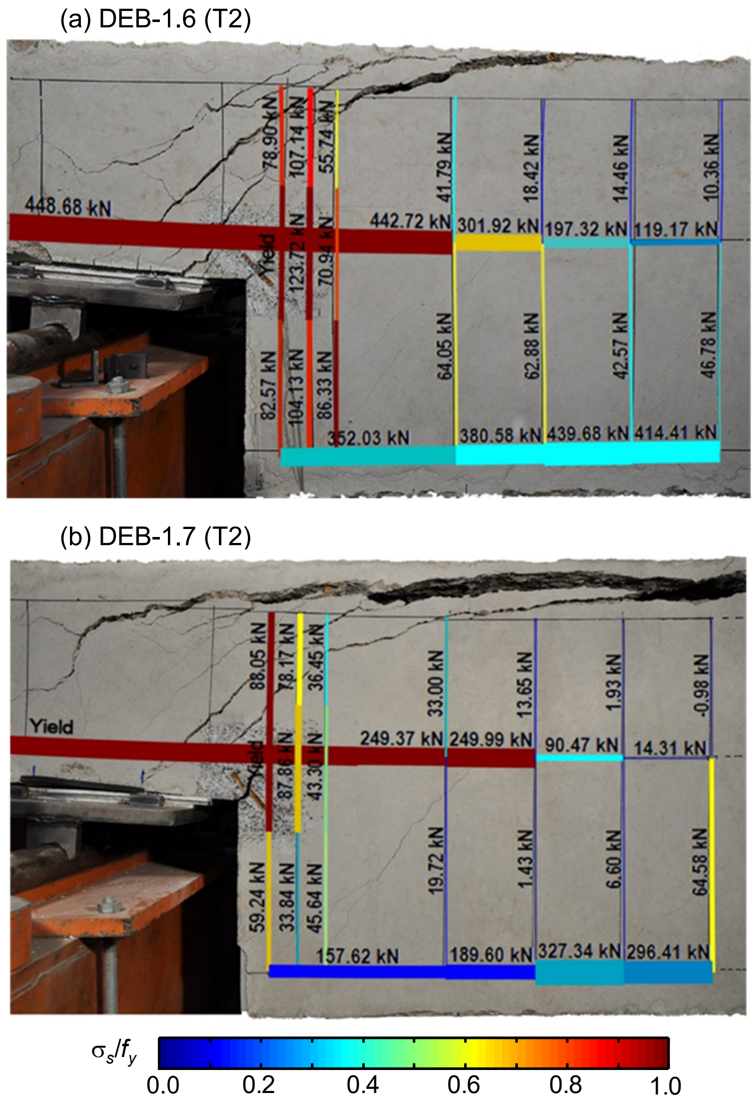

Fig. 8. Reinforcement stresses (in colour, relative to the reinforcement yield strength f_y) and tensile forces (thickness) calculated from strain measurements at peak loads.

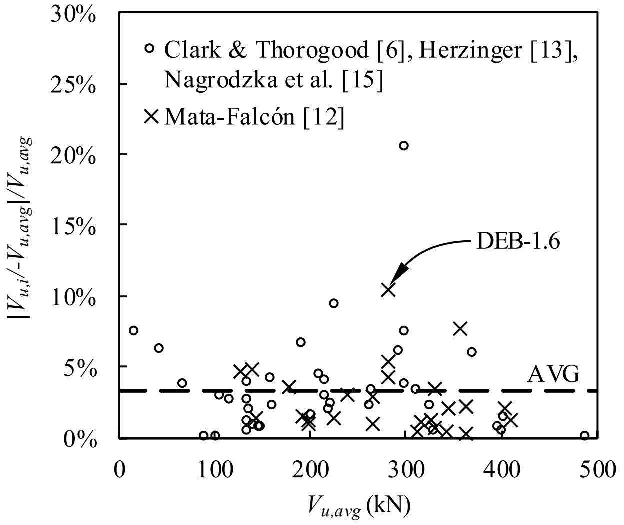

Fig. 9. Scatter between replicated tests (in the vertical axis the relative variation of the measured shear strength in each test respect to the average shear strength between replicated tests).

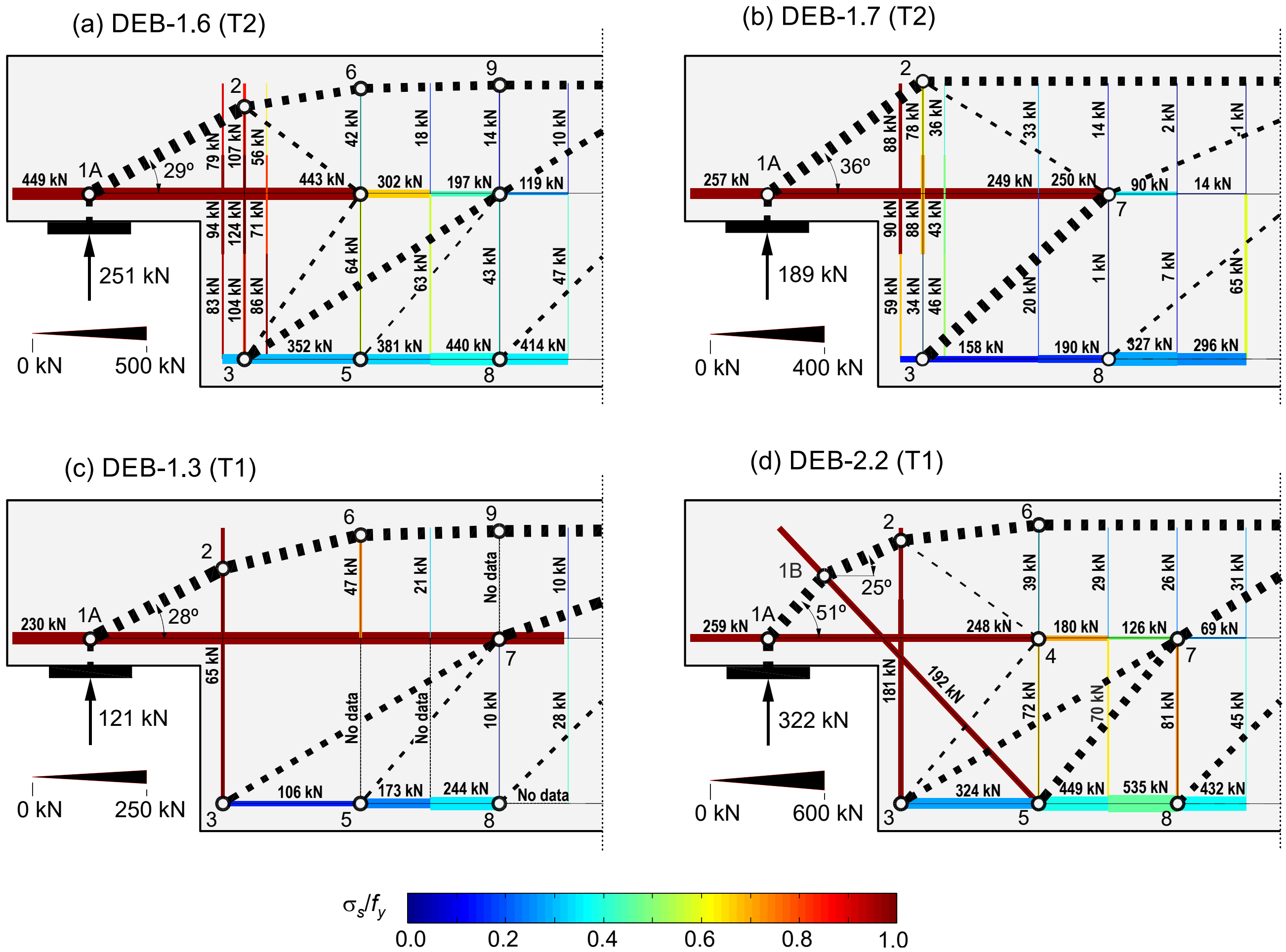

Fig. 10. Strut-and-tie models from the experimental results (struts represented in dashed black lines with a proportional thickness to their resisted loads and ties in thin continuous black lines superposed to the reinforcement experimental results – represented with colour lines and text display of the measured force of each reinforcement layer –).

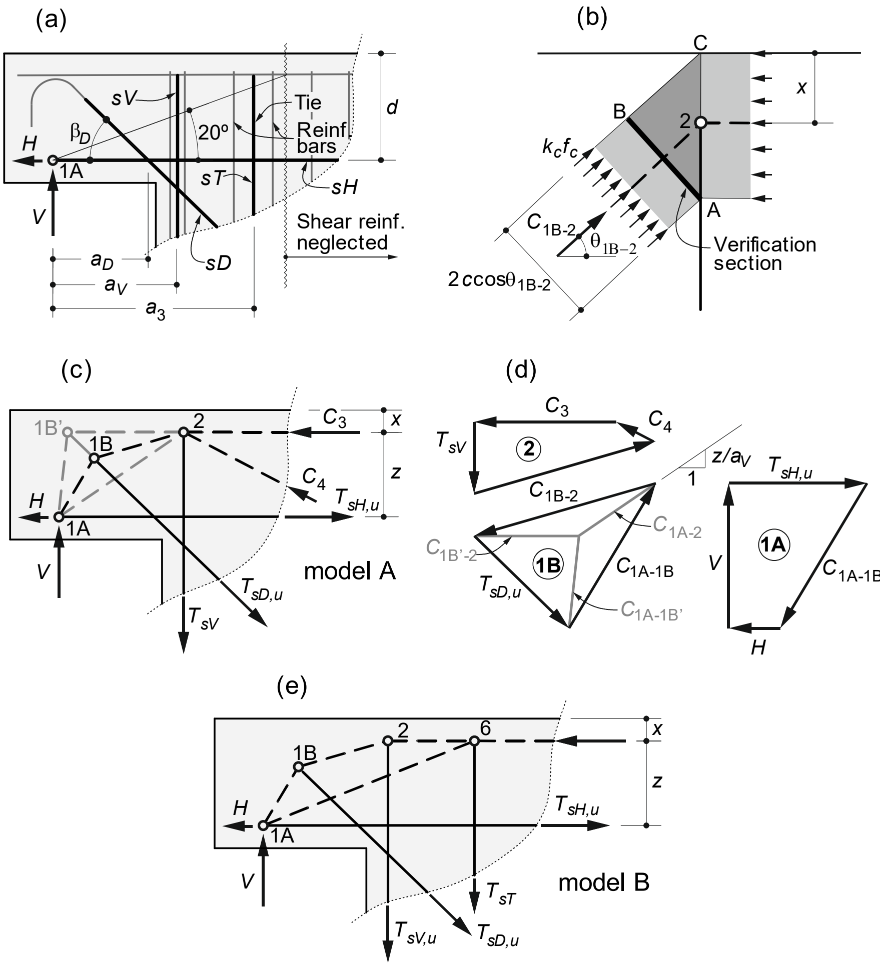

Fig. 11. Proposed simplified strut-and-tie models for dapped-end beams: (a) definition of ties; (b) node on top the hanger reinforcement and verification section; (c)-(d) model A, description and equilibrium in nodes and (e) model B.

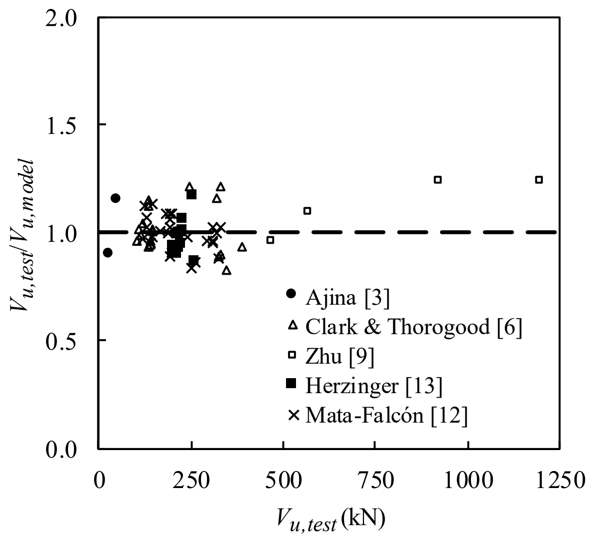

Fig. 12. Ratio between the experimental load and the load predicted by the proposed model (k_c=0.55·η_{fc}) as a function of the experimental load.

TABLES

Table 1. Properties of test specimens.

Specimen (codification)	Graphical description†	A_{sH} (mm^2)	A_{sV1} (mm^2)	A_{sV2} (mm^2)	A_{sV3} (mm^2)	A_{sD} (mm^2)	A_{s1} (mm^2)	A_{s2} (mm^2)	A_{s3} (mm^2/m)	f_c (MPa)
		Dapped-end reinforcement					Beam reinforcement			
DEB-1.1 (p49/O.1)	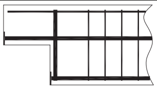	5Ø10 (393)	2Ø10+2Ø8 (258)	-	-	-	4Ø20 (1257)	-	2Ø8/0.125 (808)	41.1
DEB-1.2 (p49/O.2)	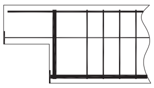	3Ø10 (236)	2Ø10+2Ø8 (258)	-	-	-	4Ø20 (1257)	-	2Ø8/0.125 (808)	39.3
DEB-1.3 (p49/O.3)	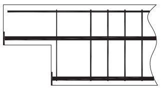	5Ø10 (393)	2Ø8 (101)	-	-	-	4Ø20 (1257)	-	2Ø8/0.125 (808)	39.9
DEB-1.4 (p49/O.1)	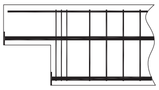	5Ø10 (393)	2Ø8 (101)	2Ø6 (57)	2Ø8 (101)	-	4Ø20 (1257)	-	2Ø8/0.125 (808)	40.4
DEB-1.5 (p49/O.2)	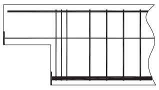	3Ø10 (236)	2Ø8 (101)	2Ø6 (57)	2Ø8 (101)	-	4Ø20 (1257)	-	2Ø8/0.125 (808)	40.8
DEB-1.6 (p100/O.1)	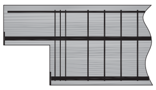	4Ø16 (804)	2Ø10 (157)	2Ø12 (226)	2Ø10 (157)	-	4Ø25 (1963)	4Ø16 (804)	4Ø8/0.125 (1608)	31.1
DEB-1.7 (p100/O.2)	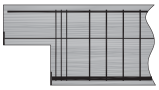	4Ø12 (452)	2Ø10 (157)	2Ø12 (226)	2Ø10 (157)	-	4Ø25 (1963)	4Ø16 (804)	4Ø8/0.125 (1608)	30.0
DEB-1.8 (p71/O.1)	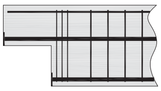	5Ø12 (565)	2Ø10 (157)	2Ø6 (57)	2Ø10 (157)	-	4Ø25 (1963)	-	2Ø8+2Ø6/0.125 (1256)	32.2
DEB-1.9 (p71/O.2)	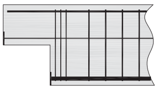	3Ø12 (339)	2Ø10 (157)	2Ø6 (57)	2Ø10 (157)	-	4Ø25 (1963)	-	2Ø8+2Ø6/0.125 (1256)	31.9
DEB-2.1 (p49/D.1)	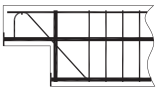	3Ø10 (236)	3Ø8 (151)	-	-	2Ø10 (157)	4Ø20 (1257)	-	2Ø8/0.125 (808)	40.2
DEB-2.2 (p100/D.1)	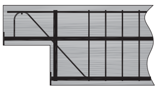	4Ø12 (452)	4Ø10 (314)	-	-	2Ø12+1Ø10 (305)	4Ø25 (1963)	4Ø16 (804)	4Ø8/0.125 (1608)	33.3
DEB-2.3 (p71/D.1)	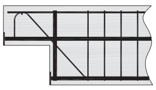	3Ø12 (339)	2Ø12 (226)	-	-	2Ø12 (226)	4Ø25 (1963)	-	2Ø8+2Ø6/0.125 (1256)	33.3
DEB-2.4 (p100/D.2)	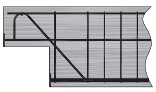	4Ø10 (314)	2Ø12 (226)	-	-	2Ø12+1Ø16 (427)	4Ø25 (1963)	4Ø16 (804)	4Ø8/0.125 (1608)	36.9
DEB-2.5 (p100/D.3)	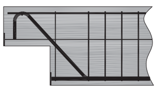	2Ø8+2Ø6 (157)	2Ø8 (101)	-	-	2Ø16+1Ø12 (515)	4Ø25 (1963)	4Ø16 (804)	4Ø8/0.125 (1608)	37.1
DEB-2.6 (p100/D.4.1)	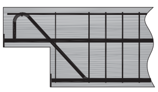	4Ø16 (804)	2Ø8 (101)	-	-	2Ø16+1Ø12 (515)	4Ø25 (1963)	4Ø16 (804)	4Ø8/0.125 (1608)	38.3

† Reinforcement sizes are not to scale. Dimensions represent only relative differences between specimens. Filling color symbolizes the amount of reinforcement as follows:

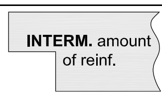

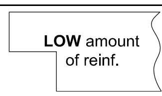

Table 2. Mechanical properties of the reinforcement.

		Reinforcement bar diameter (mm)						
		6	8	10	12	16	20	25
Specimens DEB-: 1.1, 1.2, 1.3, 1.4, 1.5, 2.1	f_y (MPa)	605.4	619.0	566.5	585.0	-	536.2	-
	f_u (MPa)	713.1	708.9	655.0	672.5	-	655.5	-
Specimens DEB-: 1.6, 1.7, 1.8, 1.9, 2.2, 2.3	f_y (MPa)	547.3	532.3	544.2	546.1	549.6	-	569.9
	f_u (MPa)	680.1	672.1	654.3	658.5	672.8	-	695.9
Specimens DEB-: 2.4, 2.5, 2.6, 3.1, 3.2, 3.3	f_y (MPa)	558.6	554.1	548.4	551.7	543.9	-	539.9
	f_u (MPa)	718.2	673.5	656.2	640.1	638.3	-	650.9

Table 3. Main results and failure modes of the experimental investigation.

Test	Spalling	Sequence of yielding	Yielding of first rebar							Peak load					
			V_y (kN)	V_y/V_u (%)	ε_{sH} (‰)	ε_{sV1} (‰)	ε_{sV2} (‰)	ε_{sV3} (‰)	ε_{sD} (‰)	V_u (kN)	ε_{sH} (‰)	ε_{sV1} (‰)	ε_{sV2} (‰)	ε_{sV3} (‰)	ε_{sD} (‰)
DEB-1.1 (T1)	Yes	*H-V*	146.3	76%	**2.93**	2.79	-	-	-	193.6	**Y**	**Y**	-	-	-
DEB-1.1 (T2)	No	*V-H*	122.0	63%	2.29	**2.95**	-	-	-	-	**Y**	**Y**	-	-	-
DEB-1.2 (T1)	Yes	*H-V*	106.1	73%	**2.84**	2.36	-	-	-	145.8	**Y**	**3.13**	-	-	-
DEB-1.2 (T2)	Yes	*H-V*	95.7	72%	**2.84**	2.49	-	-	-	132.7	**Y**	**7.92**	-	-	-
DEB-1.3 (T1)	No	*V-H*	77.5	64%	1.98	**3.10**	-	-	-	121.1	**6.35**	**Y**	-	-	-
DEB-1.3 (T2)	No	*V*	89.5	67%	1.65	**3.10**	-	-	-	133.0	2.28	**Y**	-	-	-
DEB-1.4 (T1)	Yes	*V2-V1-V3-H*	118.4	65%	2.27	2.51	**3.10**	2.98	-	183.0	**4.62**	**Y**	**Y**	**4.92**	-
DEB-1.4 (T2)	Yes	*V1-H-V2-V3*	99.5	58%	2.81	**3.10**	2.62	1.18	-	170.4	**Y**	**Y**	**Y**	**4.63**	-
DEB-1.5 (T1)	No	*H-V2-V1*	69.7	56%	**2.83**	2.66	3.01	0.80	-	125.3	**Y**	**Y**	**Y**	1.71	-
DEB-1.5 (T2)	No	*H-V1-V2*	81.2	65%	**2.80**	2.36	1.56	0.70	-	-	**Y**	**Y**	**Y**	1.64	-
DEB-1.6 (T1)	Yes	*V1-H-V2-V3*	193.4	63%	2.39	**2.72**	1.83	1.43	-	309.2	**6.18**	**Y**	**7.60**	**5.58**	-
DEB-1.6 (T2)	Yes	*V1-H-V2*	163.2	65%	1.93	**2.73**	1.71	1.33	-	250.9	**3.93**	**Y**	**2.94**	2.26	-
DEB-1.7 (T1)	No	*V1-H*	118.9	61%	1.80	**2.73**	0.80	0.95	-	194.4	**Y**	**7.04**	1.27	2.12	-
DEB-1.7 (T2)	No	*V1-H*	144.8	77%	2.56	**2.72**	1.33	1.09	-	188.8	**Y**	**Y**	1.94	1.38	-
DEB-1.8 (T1)	Yes	*V1-H-V2-V3*	126.0	65%	2.71	**2.76**	2.10	1.17	-	195.3	**Y**	**Y**	**Y**	**2.83**	-
DEB-1.8 (T2)	Yes	*H-V1-V2-V3*	94.4	47%	**2.69**	1.81	1.96	1.07	-	199.1	**Y**	**Y**	**Y**	**2.98**	-
DEB-1.9 (T1)	No	*V1-H-V2*	110.5	78%	2.25	**2.71**	2.10	0.73	-	141.7	**Y**	**Y**	**5.14**	1.26	-
DEB-1.9 (T2)	No	*V1-H-V2*	113.2	78%	2.55	**2.73**	2.37	1.29	-	145.5	**Y**	**Y**	**8.06**	1.88	-
DEB-2.1 (T1)	Yes	*D-V-H*	91.9	47%	0.90	0.85	-	-	**2.82**	194.9	**Y**	**Y**	-	-	**Y**
DEB-2.1 (T2)	Yes	*D-V-H*	104.6	52%	1.01	1.31	-	-	**2.84**	199.6	**Y**	**Y**	-	-	**Y**
DEB-2.2 (T1)	Yes	*D-V-H*	208.6	65%	1.64	1.80	-	-	**2.73**	321.8	**6.87**	**Y**	-	-	**Y**
DEB-2.2 (T2)	Yes	*D-V-H*	208.5	63%	1.42	1.40	-	-	**2.73**	329.8	**6.42**	**8.56**	-	-	**Y**
DEB-2.3 (T1)	Yes	*D-H-V*	157.3	65%	2.14	1.80	-	-	**2.88**	240.5	**Y**	**Y**	-	-	**Y**
DEB-2.4 (T1)	Yes	*D-V-H*	219.6	70%	1.88	2.01	-	-	**2.75**	311.9	**Y**	**16.2**	-	-	**Y**
DEB-2.4 (T2)	Yes	*D-V-H*	220.2	71%	1.93	2.12	-	-	**2.74**	309.4	**Y**	**8.60**	-	-	**Y**
DEB-2.5 (T1)	Yes	*H-D*	197.2	74%	**2.73**	-	-	-	2.15	265.1	**Y**	**Y**	-	-	**Y**
DEB-2.5 (T2)	Yes	*H-D-V*	208.8	71%	**2.73**	2.14	-	-	2.52	294.9	**Y**	**Y**	-	-	**Y**
DEB-2.6 (T1)	Yes	*V-D*	179.1	55%	1.00	**2.79**	-	-	1.86	328.1	2.20	**Y**	-	-	**Y**

Plastic strains are highlighted in bold; 'Y' codification represents that the strain gauges instrumentation failed before reaching the peak load having recorded plastic strains.

Table 4. Influence of the amount of reinforcement on the strength.

		$V_u/V_{u,\text{p49}}$			
Amount of reinforc.	Relative amount of reinforcement	Layout O.1	Layout O.2	Layout D.1	Avg.
p100	100/49=2.04	1.59	1.54	1.64	1.59
p71	71/49=1.45	1.11	1.15	1.21	1.16
p49	1.00	1.00	1.00	1.00	1.00

Table 5. Influence of the ratio between the horizontal and the hanger reinforcement on the strength.

		$V_u/V_{u,\mathrm{O.1}}$			
Reinf. layout	A_{sH}/A_{sV}	Amount p49	Amount p71	Amount p100	Avg.
O.1	0.67	1.00	1.00	1.00	1.00
O.2	1.12	0.71	0.73	0.68	0.71
O.3	0.27	0.66	-	-	0.66

Table 6. Forces in the strut-and-tie models proposed in Fig. 8 from the experimental results (F_h and F_v denote the horizontal and the vertical component of the force respectively; negative force represents tension).

(a) DEB-1.6 (T2)			(b) DEB-1.7 (T2)			(c) DEB-1.3 (T1)			(d) DEB-2.2 (T1)		
Strut/ Tie	F_h (kN)	F_v (kN)	Strut/ Tie	F_h (kN)	F_v (kN)	Strut/ Tie	F_h (kN)	F_v (kN)	Strut/ Tie	F_h (kN)	F_v (kN)
1A-2	449	251	1A-2	257	189	1A-2	230	121	1A-1B	259	322
2-4	121	90	2-7	53	33	2-6	230	56	1B-2	390	181
2-6	328	52	2-ext	204	0	3-7	108	65	2-4	50	36
3-4	79	112	3-7	247	221	5-7	39	47	2-6	341	36
3-7	270	176	7-ext		96	6-9	230	9	3-4	57	68
5-7	53	64	8-ext		93	7-ext		71	3-7	189	113
6-9	328	11	1-7	-257	0	8-ext		50	5-7	177	212
7-ext	-	145	2-3	0	-221	9-ext	230	0	6-7	3	3
8-ext	-	105	3-8	-247	0	1A-7	-230	0	6-ext	341	0
9-ext	328	0	7-8	0	-93	2-3	0	-65	7-ext	-	171
1A-4	-449	0				3-5	-108	0	8-ext	-	151
2-3	0	-288				5-6	0	-47	1A-4	-259	0
3-5	-349	0				5-8	-147	0	1B-5	-131	-141
4-5	0	-64				7-8	0	-50	2-3	0	-181
4-6	0	-42				7-9	0	-9	3-5	-245	0
4-7	-250	0							4-5	0	-72
5-8	-402	0							4-6	0	-39
7-8	0	-105							4-7	-153	0
									5-8	-553	0
									7-8	0	-151

Table 7. Reduction factor of the compressive strength specified in *fib* Model Code 2010 [33], EN 1992-1-1 [32] and ACI 318-14 [34] for CCT nodes with anchorage outside the nodal region and struts with oblique tension.

	CCT node			Strut with oblique tension		
f_{ck} (MPa)	ACI 318-14 k_c=0.85·0.8	EN 1992 k_c=v'·0.85	*fib* MC 2010 k_c=η_{fc}·0.75	ACI 318-14 k_c=0.85·0.6	EN 1992 k_c=v'·0.6	*fib* MC 2010 k_c=η_{fc}·0.55
20	0.68	0.78	0.75	0.51	0.55	0.55
30	0.68	0.75	0.75	0.51	0.53	0.55
40	0.68	0.71	0.68	0.51	0.50	0.50
50	0.68	0.68	0.63	0.51	0.48	0.46

Table 8. Statistical comparison of test results to proposed model for different values of the effective compressive strength (ratio V_{test}/V_{model}).

	Num. tests	*fib* MC 2010 ($k_c=\eta_{fc}\cdot 0.75$)			*fib* MC 2010 ($k_c=\eta_{fc}\cdot 0.55$)		
		Avg.	CoV	%>1.00	Avg.	CoV	%>1.00
Ajina [3]	2	1.03	0.17	50%	1.10	0.16	50%
Clark & Thorogood [6]	20	1.01	0.11	50%	1.04	0.11	50%
Zhu [9]	4	1.13	0.12	75%	1.16	0.12	75%
Herzinger [13]	13	0.97	0.08	23%	1.01	0.08	46%
Mata-Falcón [12]	26	1.00	0.08	46%	1.03	0.07	62%
ALL	65	1.00	0.10	45%	1.04	0.10	55%

Table 9. Detailed results of the proposed model and comparison to test results (f_{1c}=0.55·η_{fc}).

Author	Test	$T_{sH,u}$ (kN)	$T_{sV,u}$ (kN)	$T_{sD,u}\cdot\sin\beta_D$ (kN)	$T_{s3,u}$ (kN)	θ_{1A-2} (º)	θ_{1A-6} (º)	z/d	S&T model	$V_{u,test}$ (kN)	$H_{u,test}/V_{u,test}$	$V_{u,model}$ (kN)	$V_{u,test}/V_{u,model}$
Ajina [3]	B2	69.8	58.4	0.0	29.2	29.2	17.7	0.79	A	48.0	0.0	39.1	1.23
	B6	69.8	58.4	0.0	29.2	22.3	13.2	0.76	A	28.0	0.0	28.6	0.98
Clark & Thorogood [6]	3 (T1)	56.8	49.5	63.4	111.4	46.5	25.3	0.94	B	114.0	0.0	114.1	1.00
	3 (T2)	56.8	49.5	63.4	111.4	46.5	25.3	0.94	B	120.0	0.0	114.1	1.05
	4 (T1)	267.9	154.7	182.5	111.4	40.1	22.0	0.81	B	328.0	0.0	352.6	0.93
	4 (T2)	267.9	154.7	182.5	111.4	40.1	22.0	0.81	B	330.0	0.0	352.6	0.94
	7 (T1)	49.5	49.5	63.4	111.4	60.9	29.2	0.90	B	135.0	0.0	143.5	0.94
	7 (T2)	49.5	49.5	63.4	111.4	60.9	29.2	0.90	B	136.0	0.0	143.5	0.95
	8 (T1)	222.8	154.7	182.5	111.4	50.6	23.3	0.69	B	349.0	0.0	404.3	0.86
	8 (T2)	222.8	154.7	182.5	111.4	50.6	23.3	0.69	B	392.0	0.0	404.3	0.97
	9 (T1)	77.4	111.4	0.0	111.4	59.3	27.7	0.84	B	137.0	0.0	117.4	1.17
	9 (T2)	77.4	111.4	0.0	111.4	59.3	27.7	0.84	B	134.0	0.0	117.4	1.14
	10 (T1)	278.5	222.8	0.0	111.4	50.7	23.3	0.69	B	333.0	0.0	264.3	1.26
	10 (T2)	278.5	222.8	0.0	111.4	50.7	23.3	0.69	B	319.0	0.0	264.3	1.21
	11 (T1)	154.7	111.4	0.0	111.4	57.6	21.5	0.79	B	142.0	0.0	144.5	0.98
	11 (T2)	154.7	111.4	0.0	111.4	57.6	21.5	0.79	B	140.0	0.0	144.5	0.97
	12 (T1)	222.8	222.8	0.0	111.4	41.1	22.8	0.84	A	205.0	0.0	194.7	1.05
	12 (T2)	222.8	222.8	0.0	111.4	41.1	22.8	0.84	A	247.0	0.0	194.7	1.27
	17 (T1)	49.5	49.5	63.4	111.4	60.6	29.0	0.89	B	147.0	0.0	142.8	1.03
	17 (T2)	49.5	49.5	63.4	111.4	60.6	29.0	0.89	B	145.0	0.0	142.8	1.02
	18 (T1)	49.5	49.5	63.4	111.4	46.5	25.3	0.94	A	104.0	0.0	106.5	0.98
	18 (T2)	49.5	49.5	63.4	111.4	46.5	25.3	0.94	A	110.0	0.0	106.5	1.03
Zhu et al. [9]	T4	626.2	375.7	0.0	250.5	49.6	23.8	0.83	B	571.6	0.0	510.4	1.12
	T5	375.7	375.7	279.2	250.5	51.2	25.0	0.88	B	920.8	0.0	727.7	1.27
	T6	375.7	626.2	0.0	250.5	51.6	25.3	0.89	A	467.1	0.0	474.1	0.99
	T7	375.7	375.7	465.4	250.5	51.2	25.0	0.88	B	1196.6	0.0	945.7	1.27
Herzinger [13]	DE-A-1.0 (T1)	300.6	172.0	0.0	86.0	44.8	24.3	0.75	B	216.0	0.2	210.0	1.03
	DE-A-1.0 (T2)	300.6	172.0	0.0	86.0	45.9	25.2	0.78	B	255.0	0.2	211.0	1.21
	DE-A-0.5 (T1)	300.6	172.0	0.0	86.0	44.9	24.4	0.76	B	231.0	0.2	208.9	1.11
	DE-B-1.0 (T1)	359.5	145.6	0.0	86.0	43.9	22.2	0.71	B	203.0	0.2	214.0	0.95
	DE-B-1.0 (T2)	359.5	145.6	0.0	86.0	44.3	22.4	0.71	B	226.0	0.2	213.7	1.06
	DE-B-0.5 (T1)	359.5	145.6	0.0	86.0	43.6	21.9	0.70	B	205.0	0.2	212.4	0.97
	DE-B-0.5 (T2)	359.5	145.6	0.0	86.0	43.7	22.0	0.70	B	222.0	0.2	211.4	1.05
	DE-C*-1.0 (T1)	86.0	86.0	243.5	86.0	52.3	29.2	0.89	A	260.0	0.2	290.0	0.90
	DE-D-1.0 (T1)	202.3	72.8	100.0	86.0	48.6	23.1	0.83	B	220.0	0.2	229.9	0.96
	DE-Du-1.0 (T1)	202.3	72.8	100.0	86.0	48.3	22.9	0.82	B	213.0	0.2	229.5	0.93
	DE-Du-1.0 (T2)	202.3	72.8	100.0	86.0	48.5	23.0	0.83	B	222.0	0.2	229.1	0.97
	DE-D*-1.0 (T1)	127.2	63.5	114.7	86.0	51.4	25.9	0.89	B	214.0	0.2	210.9	1.01
	DE-D*-1.0 (T2)	127.2	63.5	114.7	86.0	51.4	25.9	0.89	B	203.0	0.2	212.5	0.96
Mata-Falcón [12]	DEB-1.1 (T1)	222.5	151.2	0.0	62.2	41.7	23.5	0.85	B	193.6	0.0	174.1	1.11
	DEB-1.2 (T1)	133.5	151.2	0.0	62.2	43.3	24.8	0.91	A	145.8	0.0	125.9	1.16
	DEB-1.2 (T2)	133.5	151.2	0.0	62.2	43.3	24.8	0.91	A	132.7	0.0	125.9	1.05
	DEB-1.3 (T1)	222.5	62.2	0.0	62.2	41.6	23.5	0.85	B	121.1	0.0	124.5	0.97
	DEB-1.3 (T2)	222.5	62.2	0.0	62.2	41.6	23.5	0.85	B	133.0	0.0	124.5	1.07
	DEB-1.4 (T1)	222.5	155.4	0.0	62.2	37.8	23.9	0.87	B	183.0	0.0	165.2	1.11
	DEB-1.4 (T2)	222.5	155.4	0.0	62.2	37.8	23.9	0.87	B	170.4	0.0	165.2	1.03
	DEB-1.5 (T1)	133.5	155.4	0.0	62.2	39.3	25.1	0.92	A	125.3	0.0	109.4	1.15
	DEB-1.6 (T1)	442.0	294.5	0.0	107.0	32.4	19.9	0.71	A	309.2	0.0	280.3	1.10
	DEB-1.6 (T2)	442.0	294.5	0.0	107.0	32.4	19.9	0.71	A	250.9	0.0	280.3	0.90
	DEB-1.7 (T1)	247.0	294.5	0.0	107.0	36.1	22.6	0.82	A	194.4	0.0	180.1	1.08
	DEB-1.7 (T2)	247.0	294.5	0.0	107.0	36.1	22.6	0.82	A	188.8	0.0	180.1	1.05
	DEB-1.8 (T1)	308.8	201.9	0.0	84.5	35.2	22.0	0.79	B	195.3	0.0	211.1	0.92
	DEB-1.8 (T2)	308.8	201.9	0.0	84.5	35.2	22.0	0.79	B	199.1	0.0	211.1	0.94
	DEB-1.9 (T1)	185.3	201.9	0.0	84.5	37.7	23.8	0.87	A	141.7	0.0	143.1	0.99

DEB-1.9 (T2)	185.3	201.9	0.0	84.5	37.7	23.8	0.87	A	145.5	0.0	143.1	1.02
DEB-2.1 (T1)	133.5	93.3	65.1	62.2	43.1	24.6	0.90	B	194.9	0.0	180.8	1.08
DEB-2.1 (T2)	133.5	93.3	65.1	62.2	43.1	24.6	0.90	B	199.6	0.0	180.8	1.10
DEB-2.2 (T1)	247.0	171.0	121.6	107.0	39.7	22.1	0.80	B	321.8	0.0	309.3	1.04
DEB-2.2 (T2)	247.0	171.0	121.6	107.0	39.7	22.1	0.80	B	329.8	0.0	309.3	1.07
DEB-2.3 (T1)	185.3	123.5	90.3	84.5	41.3	23.3	0.84	B	240.5	0.0	238.8	1.01
DEB-2.4 (T1)	172.3	124.8	171.3	111.4	41.4	23.3	0.85	B	311.9	0.0	313.7	0.99
DEB-2.4 (T2)	172.3	124.8	171.3	111.4	41.4	23.3	0.85	B	309.4	0.0	313.7	0.99
DEB-2.5 (T1)	87.3	55.7	205.6	111.4	42.6	24.2	0.88	B	265.1	0.0	295.5	0.90
DEB-2.5 (T2)	87.3	55.7	205.6	111.4	42.6	24.2	0.88	B	294.9	0.0	295.5	1.00
DEB-2.6 (T1)	437.4	55.7	205.6	111.4	36.5	19.9	0.71	B	328.1	0.0	372.7	0.88